

# A Novel Sixth Order Energy-Conserved Method for Three-Dimensional Time-Domain Maxwell's Equations

Chaolong Jiang<sup>1</sup>, Wenjun Cai<sup>1</sup>, Yushun Wang<sup>1,\*</sup>, Haochen Li<sup>2</sup>

<sup>1</sup> Jiangsu Provincial Key Laboratory for NSLSCS,  
School of Mathematical Sciences, Nanjing Normal University,  
Nanjing 210023, China

<sup>2</sup> LMAM, CAPT and School of Mathematical Sciences,  
Peking University, Beijing 100871, China

## Abstract

In this paper, a novel sixth order energy-conserved method is proposed for solving the three-dimensional time-domain Maxwell's equations. The new scheme preserves five discrete energy conservation laws, three momentum conservation laws, symplectic conservation law as well as two divergence-free properties and is proved to be unconditionally stable, non-dissipative. An optimal error estimate is established based on the energy method, which shows that the proposed method is of sixth order accuracy in time and spectral accuracy in space in discrete  $L^2$ -norm. The constant in the error estimate is proved to be only  $O(T)$ . Furthermore, the numerical dispersion relation is analyzed in detail and a fast solver is presented to solve the resulting discrete linear equations efficiently. Numerical results are addressed to verify our theoretical analysis.

**AMS subject classification:** 65M12, 65M15, 65M70

**Keywords:** Maxwell's equations, average vector field method, error estimate, dispersion relation, divergence preservation, conservation laws.

## 1 Introduction

The Maxwell's equations describe the propagation and scattering of electromagnetic waves and have a wide variety of applications in science and engineering, including microwave circuits, radio-frequency, antennas, aircraft radar, integrated optical circuits, wireless engineering, etc. Various applications stimulate the investigation on the construction of efficient numerical methods for the Maxwell's equations. A well-known numerical method in computational electromagnetic is the finite-difference time domain (FDTD) method, which was first introduced by Yee [47] and further developed and analyzed in Refs. [34, 44]. However, the Yee-based FDTD method is only conditionally stable so that it may require very small temporal step-size and suffer impractical computational cost for long time computation.

In recent years, due to the superior properties in long time numerical computation over traditional numerical methods, structure-preserving methods have been proved to be very powerful in numerical simulations (e.g., see Refs. [17, 20, 26, 30] and references therein). As one of the most important components of the structure-preserving methods, symplectic schemes, which can preserve the symplectic conservation law of the Maxwell's equations, have gained remarkable success in the numerical analysis of the

---

\*Correspondence author. Email: wangyushun@njnu.edu.cn.

Maxwell's equations (e.g., see Refs. [7, 21, 25, 40, 42, 43, 51] and references therein). In addition to the symplectic conservation law, the Maxwell's equations also admit two divergence-free fields, five energy conservation laws and three momentum conservation laws, which are very important invariants for long time propagation of the electromagnetic waves [44]. Thus, devising the numerical schemes, which can inherit these original physical features as much as possible, attracts a lot of interest. In Ref. [13], Chen et al. proposed an energy-conserved splitting scheme for two dimensional (2D) Maxwell's equations in an isotropic, lossless and sourceless medium. Further analysis in three dimensional (3D) case was investigated in Ref. [14]. Other energy-conserved splitting schemes can be found in Refs. [22, 25, 28]. However, most of existing energy-conserved splitting schemes have only second order accuracy in both time and space at most. The second order schemes are usually effective for geometries of moderate electrical size, but, for computing large scale problems, for problems requiring long-time integration, or for problems of wave propagations over longer distances, it is indispensable for the development of higher order schemes which produce smaller dispersion or phase errors for a given mesh resolution [28].

In fact, various spatial high order methods have been proposed for the Maxwell's equations in the literature, such as the high order FDTD methods (e.g., Refs. [38, 41, 44, 48, 49]), the Finite element method (see the monograph [33]) and the Fourier pseudo-spectral method [29]. However, most of these methods have only second order accuracy in time to the best of our knowledge. In Ref. [5], with the aid of the splitting techniques, an unconditionally stable energy-conserved scheme was presented. This scheme has fourth order accuracy in time and spectral accuracy in space, respectively. Higher order methods can be constructed by using the splitting techniques, however, this approach can be tedious in practice computation and error estimate. In addition, the scheme cannot preserve the two discrete divergence-free fields. The resulting large divergence-free errors may make the predicted solutions less stable in long time simulations of the electromagnetic wave propagation. Avoidance of this numerical instability is critical in the development of an effective numerical method for the Maxwell's equations [15, 35]. Subsequently, another energy-conserved scheme with fourth order accuracy in time and spectral accuracy in space, respectively, was designed in Ref. [6]. The scheme can preserve the two discrete divergence-free fields of the Maxwell's equations. However, there has been no reference considering a sixth order energy-conserved method for the 3D Maxwell's equations.

Thus, in this paper, our main contributions are as follows:

1. We first propose a sixth order energy-conserved scheme for the three-dimensional time-domain Maxwell's equations, which satisfies the following properties.
  - The proposed scheme is unconditionally stable and non-dissipative (numerical dispersion analysis).
  - The proposed scheme is symmetric and can preserve five energy, three momentum conservation laws, symplectic conservation law as well as two discrete divergence-free fields.
2. An optimal error estimate of the proposed scheme is established, which shows that the proposed scheme is unconditionally convergent with order of  $O(\tau^6 + N^{-r})$  in discrete  $L^2$ -norm, where  $\tau$  is the time step size and  $N$  is the collocation points used in the spectral method. In particular, the constant in the error estimate is only  $O(T)$ .
3. The numerical dispersion relation including the phase velocity and the group velocity of the scheme is analyzed in detail, which gives two novel results:

- The extra solution branches of the Fourier pseudo-spectral scheme only occur with large wave numbers.
  - The grid-anisotropy of the Fourier pseudo-spectral scheme is direction-independent.
4. A fast solver is developed for solving the resulting linear equations efficiently, which can be extended directly to other literature (e.g., Refs. [6, 51]).

The outline of this paper is organized as follows. In Section 2, the Hamiltonian structures of the Maxwell's equations as well as the conservation laws in continuous sense is introduced. A sixth order energy-conserved scheme for the Maxwell's equations is proposed in Section 3. The discrete conservation laws including the five energy conservation laws, the three momentum conservation laws, the symplecticity and the two divergence-free fields are rigorously proved in Section 4. The convergence is analyzed in Section 5. Numerical dispersion relation is investigated in Section 6. In Section 7, numerical experiments are presented. We draw some conclusions in Section 8. Finally, a fast solver is presented in Appendix.

## 2 Hamiltonian structures and conservation laws

In this section, we will introduce the Hamiltonian structures of the Maxwell's equations as well as the conservation laws in continuous sense.

The 3D time-domain Maxwell's equations in an isotropic, lossless and sourceless medium can be written as

$$\begin{cases} \frac{\partial \mathbf{E}}{\partial t} = \frac{1}{\epsilon} \nabla \times \mathbf{H}, \\ \frac{\partial \mathbf{H}}{\partial t} = -\frac{1}{\mu} \nabla \times \mathbf{E}, \\ \nabla \cdot (\epsilon \mathbf{E}) = 0, \\ \nabla \cdot (\mu \mathbf{H}) = 0, \end{cases} \quad (2.1)$$

where  $\mathbf{E} = (E_x, E_y, E_z)^T$  is the electric field intensity,  $\mathbf{H} = (H_x, H_y, H_z)^T$  is the magnetic field intensity, constant scalars  $\mu$  and  $\epsilon$  are the magnetic permeability and the electric permittivity, respectively. Here, we assume the periodic boundary conditions (PBCs) on the boundary of the cuboid domain  $\Omega = [x_L, x_R] \times [y_L, y_R] \times [z_L, z_R]$ . The initial conditions are supposed to be

$$\mathbf{E}(x, y, z, 0) = \mathbf{E}_0(x, y, z), \quad \mathbf{H}(x, y, z, 0) = \mathbf{H}_0(x, y, z), \quad (x, y, z) \in \Omega. \quad (2.2)$$

In general, the perfect electric conducting (PEC) boundary conditions are used on  $\Omega \times [0, T]$ . However, with the aid of the Bérenger's PML technique [3, 4], the periodic boundary conditions are valid in practical computations. More importantly, when the periodic boundary conditions are considered, the spatial derivatives of the Maxwell's equations can be efficiently computed by using the fast Fourier transform (FFT). For more details, please refer to Ref. [29].

The Maxwell's equations (2.1) are a bi-Hamiltonian system, which implies that there are two infinite-dimensional Hamiltonian formulations.

The first one is given by

$$\frac{\partial}{\partial t} \begin{pmatrix} \mathbf{H} \\ \mathbf{E} \end{pmatrix} = \begin{pmatrix} 0 & -\mathbf{I}_{3 \times 3} \\ \mathbf{I}_{3 \times 3} & 0 \end{pmatrix} \begin{pmatrix} \epsilon^{-1} \nabla \times \mathbf{H} \\ \mu^{-1} \nabla \times \mathbf{E} \end{pmatrix} = \mathcal{J}_1 \left( \begin{pmatrix} \frac{\delta \mathcal{H}_1}{\delta \mathbf{H}} \\ \frac{\delta \mathcal{H}_1}{\delta \mathbf{E}} \end{pmatrix} \right), \quad (2.3)$$

with the helicity Hamiltonian functional [1]

$$\mathcal{H}_1 = \int_{\Omega} \left( \frac{1}{2\epsilon} \mathbf{H}^T (\nabla \times \mathbf{H}) + \frac{1}{2\mu} \mathbf{E}^T (\nabla \times \mathbf{E}) \right) dx dy dz. \quad (2.4)$$

The other one reads

$$\frac{\partial}{\partial t} \begin{pmatrix} \mathbf{H} \\ \mathbf{E} \end{pmatrix} = \begin{pmatrix} 0 & -(\epsilon\mu)^{-1} \nabla \times \\ (\epsilon\mu)^{-1} \nabla \times & 0 \end{pmatrix} \begin{pmatrix} \mu \mathbf{H} \\ \epsilon \mathbf{E} \end{pmatrix} = \mathcal{J}_2 \begin{pmatrix} \frac{\delta \mathcal{H}_2}{\delta \mathbf{H}} \\ \frac{\delta \mathcal{H}_2}{\delta \mathbf{E}} \end{pmatrix}, \quad (2.5)$$

where the quadratic Hamiltonian functional yields [31]

$$\mathcal{H}_2 = \int_{\Omega} \left( \frac{\mu}{2} \mathbf{H}^T \mathbf{H} + \frac{\epsilon}{2} \mathbf{E}^T \mathbf{E} \right) dx dy dz, \quad (2.6)$$

which is the electromagnetic energy in the Poynting theorem in classical electromagnetism [24].

With the Hamiltonian formulations (2.3) and (2.5), the Maxwell's equations (2.1) satisfy the symplectic, the helicity and quadratic conservation laws.

**Lemma 2.1.** [43] *Let  $\mathbf{H}$  and  $\mathbf{E}$  be the solutions of the Maxwell's equations (2.1) and satisfy PBCs, then it holds that*

$$\frac{d}{dt} \int_{\Omega} \omega(x, y, z, t) dx dy dz = 0, \quad \omega = dE_x \wedge dH_x + dE_y \wedge dH_y + dE_z \wedge dH_z. \quad (2.7)$$

**Lemma 2.2.** [43] *Let  $\mathbf{H}$  and  $\mathbf{E}$  be the solutions of the Maxwell's equations (2.1) and satisfy PBCs, then the helicity and quadratic conservation laws hold, i.e.,*

$$\frac{d}{dt} \int_{\Omega} \left( \frac{1}{2\epsilon} \mathbf{H}^T (\nabla \times \mathbf{H}) + \frac{1}{2\mu} \mathbf{E}^T (\nabla \times \mathbf{E}) \right) dx dy dz = 0, \quad (2.8)$$

$$\frac{d}{dt} \int_{\Omega} \left( \frac{\mu}{2} \mathbf{H}^T \mathbf{H} + \frac{\epsilon}{2} \mathbf{E}^T \mathbf{E} \right) dx dy dz = 0. \quad (2.9)$$

Additionally, the Maxwell's equations (2.1) also admit others conservation laws.

**Lemma 2.3.** [43] *Let  $\mathbf{H}$  and  $\mathbf{E}$  be the solutions of the Maxwell's equations (2.1) and satisfy PBCs, then there exist the momentum conservation laws*

$$\frac{d}{dt} \int_{\Omega} \mathbf{H}^T \partial_w \mathbf{E} dx dy dz = 0, \quad (2.10)$$

where  $w = x, y, \text{ or } z$ , and hereafter.

**Lemma 2.4.** [18] *Let  $\mathbf{H}$  and  $\mathbf{E}$  be the solutions of the Maxwell's equations (2.1) and satisfy PBCs, then there admit the energy conservation laws*

$$\frac{d}{dt} \int_{\Omega} \left( \frac{\epsilon}{2} \partial_t \mathbf{E}^T \partial_t \mathbf{E} + \frac{\mu}{2} \partial_t \mathbf{H}^T \partial_t \mathbf{H} \right) dx dy dz = 0, \quad (2.11)$$

$$\frac{d}{dt} \int_{\Omega} \left( \epsilon \partial_w \mathbf{E}^T \partial_w \mathbf{E} + \mu \partial_w \mathbf{H}^T \partial_w \mathbf{H} \right) dx dy dz = 0, \quad (2.12)$$

$$\frac{d}{dt} \int_{\Omega} \left( \epsilon \partial_{tw} \mathbf{E}^T \partial_{tw} \mathbf{E} + \mu \partial_{tw} \mathbf{H}^T \partial_{tw} \mathbf{H} \right) dx dy dz = 0. \quad (2.13)$$

### 3 A sixth order energy-conserved scheme

In this section, our main goal is to propose a sixth order energy-conserved method for the Maxwell's equations in time. Let  $\Omega_h = \{(x_j, y_k, z_m) | x_j = x_L + (j-1)h_x, y_k = y_L + (k-1)h_y, z_m = z_L + (m-1)h_z; j = 1, \dots, N_x, k = 1, \dots, N_y, m = 1, \dots, N_z\}$  be a partition of  $\Omega$  with the mesh size  $h_w = \frac{L_w}{N_w}$ , where  $N_w$  is an even integers and  $L_w = w_R - w_L$ . Denote  $h = \max\{h_x, h_y, h_z\}$ . Let  $\Omega_\tau = \{t_n | t_n = n\tau; 0 \leq n \leq M\}$  be a uniform partition of  $[0, T]$  with the time step  $\tau = \frac{T}{M}$  and  $\Omega_{h\tau} = \Omega_h \times \Omega_\tau$ .

Let  $\{U_{j,k,m}^n | j = 1, \dots, N_x, k = 1, \dots, N_y, m = 1, \dots, N_z, 0 \leq n \leq M\}$  be a mesh functions defined on  $\Omega_{h\tau}$ . Some notations are introduced below.

$$\hat{\delta}_t U_{j,k,m}^{n-1/2} = \frac{U_{j,k,m}^n - U_{j,k,m}^{n-1}}{\tau}, \quad U_{j,k,m}^{n+\frac{1}{2}} = \frac{U_{j,k,m}^{n+1} + U_{j,k,m}^n}{2}.$$

Moreover, for any grid functions  $U_{j,k,m}, V_{j,k,m}, (x_j, y_k, z_m) \in \Omega_h$ , we define the inner product and the norm by

$$\langle \mathbf{U}, \mathbf{V} \rangle_h = h_x h_y h_z \sum_{j=1}^{N_x} \sum_{k=1}^{N_y} \sum_{m=1}^{N_z} U_{j,k,m} \bar{V}_{j,k,m}, \quad \|\mathbf{U}\|_h^2 = \langle \mathbf{U}, \mathbf{U} \rangle_h, \quad \|\mathbf{U}\|_{h,\infty} = \max_{j,k,m} |U_{j,k,m}|,$$

where  $\bar{V}_{j,k,m}$  denotes the conjugate of  $V_{j,k,m}$ . For vectors  $\mathbf{U} = [(U_x)^T, (U_y)^T, (U_z)^T]^T$  and  $\mathbf{V} = [(V_x)^T, (V_y)^T, (V_z)^T]^T$ , the corresponding inner product and norm are

$$\begin{aligned} \langle \mathbf{U}, \mathbf{V} \rangle_h &= \langle U_x, V_x \rangle_h + \langle U_y, V_y \rangle_h + \langle U_z, V_z \rangle_h, \\ \|\mathbf{U}\|_h^2 &= \langle U_x, U_x \rangle_h + \langle U_y, U_y \rangle_h + \langle U_z, U_z \rangle_h. \end{aligned}$$

#### 3.1 Fourier pseudo-spectral approximation in space

As achieving high order accuracy in time, we should also treat the space with an appropriate discretization. The Fourier pseudo-spectral method is a very good candidate because of the high order accuracy and the fast Fourier transform (FFT) algorithm. Moreover, it is shown that the Fourier pseudo-spectral method exhibits obvious superiority over the conventional finite difference method in simulating electromagnetic waves [29].

Now, let us introduce the following Fourier pseudo-spectral discretization for the space variables. We define

$$S_N''' = \text{span}\{g_j(x)g_k(y)g_m(z), j = 1, \dots, N_x, k = 1, \dots, N_y, m = 1, \dots, N_z\},$$

as the interpolation space, where  $g_j(x)$ ,  $g_k(y)$  and  $g_m(z)$  are trigonometric polynomials of degree  $N_x/2$ ,  $N_y/2$  and  $N_z/2$ , given respectively by

$$\begin{aligned} g_j(x) &= \frac{1}{N_x} \sum_{l=-N_x/2}^{N_x/2} \frac{1}{a_l} e^{il\mu_x(x-x_j)}, \quad g_k(y) = \frac{1}{N_y} \sum_{s=-N_y/2}^{N_y/2} \frac{1}{b_s} e^{is\mu_y(y-y_k)}, \\ g_m(z) &= \frac{1}{N_z} \sum_{q=-N_z/2}^{N_z/2} \frac{1}{c_q} e^{iq\mu_z(z-z_m)}, \end{aligned}$$

$$\text{with } a_l = \begin{cases} 1, & |l| < \frac{N_x}{2}, \\ 2, & |l| = \frac{N_x}{2}, \end{cases}, \quad b_p = \begin{cases} 1, & |s| < \frac{N_y}{2}, \\ 2, & |s| = \frac{N_y}{2}, \end{cases}, \quad c_q = \begin{cases} 1, & |q| < \frac{N_z}{2}, \\ 2, & |q| = \frac{N_z}{2}, \end{cases} \quad \text{and } \mu_w = \frac{2\pi}{L_w}.$$

We define the interpolation operator  $I_N : C(\Omega) \rightarrow S_N'''$  as follows

$$I_N U(x, y, z, t) = \sum_{j=1}^{N_x} \sum_{k=1}^{N_y} \sum_{m=1}^{N_z} U_{j,k,m}(t) g_j(x) g_k(y) g_m(z), \quad (3.1)$$

where  $U_{j,k,m}(t) = U(x_j, y_k, z_m, t)$  and its vector form is denoted by

$$\mathbf{U} = (U_{1,1,1}, \dots, U_{N_x,1,1}, U_{1,2,1}, \dots, U_{N_x,2,1}, \dots, U_{1,N_y,N_z}, \dots, U_{N_x,N_y,N_z})^T.$$

Making partial differential with respect to  $x$ ,  $y$  and  $z$ , respectively, and evaluating the resulting expression at collocation points  $(x_j, y_k, z_m)$ , we can obtain

$$\begin{aligned} \frac{\partial^p I_N U(x_j, y_k, z_m, t)}{\partial x^p} &= \sum_{j'=1}^{N_x} \sum_{k'=1}^{N_y} \sum_{m'=1}^{N_z} U_{j',k',m'}(t) \frac{d^p g_{j'}(x_j)}{dx^p} g_{k'}(y_k) g_{m'}(z_m) \\ &= [(\mathbf{I}_{N_z} \otimes \mathbf{I}_{N_y} \otimes \mathbf{D}_p^x) \mathbf{U}]_{N_x N_y (m-1) + N_x (k-1) + j}, \\ \frac{\partial^p I_N U(x_j, y_k, z_m, t)}{\partial y^p} &= \sum_{j'=1}^{N_x} \sum_{k'=1}^{N_y} \sum_{m'=1}^{N_z} U_{j',k',m'}(t) g_{j'}(x_j) \frac{d^p g_{k'}(y_k)}{dy^p} g_{m'}(z_m) \\ &= [(\mathbf{I}_{N_z} \otimes \mathbf{D}_p^y \otimes \mathbf{I}_{N_x}) \mathbf{U}]_{N_x N_y (m-1) + N_x (k-1) + j}, \\ \frac{\partial^p I_N U(x_j, y_k, z_m, t)}{\partial z^p} &= \sum_{j'=1}^{N_x} \sum_{k'=1}^{N_y} \sum_{m'=1}^{N_z} U_{j',k',m'}(t) g_{j'}(x_j) g_{k'}(y_k) \frac{d^p g_{m'}(z_m)}{dz^p} \\ &= [(\mathbf{D}_p^z \otimes \mathbf{I}_{N_y} \otimes \mathbf{I}_{N_x}) \mathbf{U}]_{N_x N_y (m-1) + N_x (k-1) + j}, \end{aligned}$$

where  $\otimes$  is the Kronecker product,  $\mathbf{I}_{N_w}$  is the identity matrix of dimension  $N_w \times N_w$  and  $\mathbf{D}_p^w \in \mathbb{R}^{N_w \times N_w}$  is the spectral differential matrix whose entries are

$$(\mathbf{D}_p^w)_{j,l} = \frac{d^p g_l(w_j)}{dw^p}. \quad (3.2)$$

with  $j, l = 1, \dots, N_w$ . In fact, by careful calculations, one can obtain explicitly

$$\begin{aligned} (\mathbf{D}_1^x)_{j,l} &= \begin{cases} \frac{1}{2} \mu_x (-1)^{j+l} \cot(r_x), & j \neq l, \\ 0, & j = l, \end{cases} \\ (\mathbf{D}_2^x)_{j,l} &= \begin{cases} \frac{1}{2} \mu_x^2 (-1)^{j+l+1} \csc^2(r_x), & j \neq l, \\ -\mu_w^2 \frac{N_x^2 + 2}{12}, & j = l, \end{cases} \\ (\mathbf{D}_3^x)_{j,l} &= \begin{cases} \frac{3\mu_x^3}{4} (-1)^{j+l} \cos(r_x) \csc^3(r_x) + \frac{\mu_x^3 N_x^2}{8} (-1)^{j+l+1} \cot(r_x), & j \neq l, \\ 0, & j = l, \end{cases} \\ (\mathbf{D}_4^x)_{j,l} &= \begin{cases} \mu_w^4 (-1)^{j+l} \csc^2(r_x) \left( \frac{N_x^2}{4} - \frac{1}{2} - \frac{3}{2} \cot^2(r_x) \right), & j \neq l, \\ \mu_w^4 \left( \frac{N_x^4}{80} + \frac{N_x^2}{12} - \frac{1}{30} \right), & j = l, \end{cases} \end{aligned}$$

and

$$(\mathbf{D}_5^x)_{j,l} = \begin{cases} \frac{\mu_x^5}{32} (-1)^{j+l} \cot(r_x) \left[ N_x^4 + 20 \csc^2(r_x) (4 + 6 \cot^2(r_x) - N_x^2) \right], & j \neq l, \\ 0, & j = l, \end{cases}$$

where  $r_x = \mu_x \frac{x_j - x_l}{2}$  and  $j, l = 1, \dots, N_x$ .

Furthermore, the following relationship holds [12]

$$(\mathbf{D}_p^x)_{j,l} = ((\mathbf{D}_1^x)^p)_{j,l} + (-1)^{j+l} \frac{\mu_x^p}{2N_x} \left[ \left( i \frac{N_x}{2} \right)^p + \left( -i \frac{N_x}{2} \right)^p \right], \quad (3.3)$$

which implies that  $\mathbf{D}_p^x = (\mathbf{D}_1^x)^p$ , if  $p$  is an odd integer. Here, we only give the case of  $w = x$ . The cases of  $w = y, z$  are analogous.

**Lemma 3.1.** For a positive integer  $p$ ,  $\mathbf{D}_p^w$  has following properties

1.  $\mathbf{D}_{2p}^w$  is symmetric and the elements of  $\mathbf{D}_{2p}^w$  satisfy

$$(D_{2p}^w)_{k,k+m} = (D_{2p}^w)_{k,k-m}, \quad (D_{2p}^w)_{k,m+N_w} = (D_{2p}^w)_{k,m},$$

where  $k, m = 1, \dots, N_w$ .

2.  $\mathbf{D}_{2p-1}^w$  is skew-symmetric and the elements of  $\mathbf{D}_{2p-1}^w$  satisfy

$$(D_{2p-1}^w)_{k,k+N_w/2} = 0, \quad (D_{2p-1}^w)_{k,k+m} = -(D_{2p-1}^w)_{k,k-m}, \quad (D_{2p-1}^w)_{k,m+N_w} = (D_{2p-1}^w)_{k,m},$$

where  $k, m = 1, \dots, N_w$ .

**Proof.** Here, we only present the proof for the case of  $w = x$ . The proofs for the cases of  $w = y, z$  are analogous. By careful calculation, we can obtain

$$\frac{d^p g_j(x)}{dx^p} = \begin{cases} \frac{2(i\mu_x)^p}{N_x} \sum_{l=1}^{N_x/2} \frac{l^p}{a_l} \cos(l\mu_x(x - x_j)), & p \text{ is an even integer,} \\ \frac{2i(i\mu_x)^p}{N_x} \sum_{l=1}^{N_x/2} \frac{l^p}{a_l} \sin(l\mu_x(x - x_j)), & p \text{ is an odd integer,} \end{cases} \quad (3.4)$$

which implies that

$$(\mathbf{D}_p^x)_{j,k} = \begin{cases} \frac{2(i\mu_x)^p}{N_x} \sum_{l=1}^{N_x/2} \frac{l^p}{a_l} \cos\left((j-k) \frac{2\pi l}{N_x}\right), & p \text{ is an even integer,} \\ \frac{2i(i\mu_x)^p}{N_x} \sum_{l=1}^{N_x/2} \frac{l^p}{a_l} \sin\left((j-k) \frac{2\pi l}{N_x}\right), & p \text{ is an odd integer.} \end{cases} \quad (3.5)$$

By simple calculation, we finish the proof.  $\square$

**Lemma 3.2.** For a positive integer  $p$ ,  $(\mathbf{D}_1^w)^p$  has the properties

1.  $(\mathbf{D}_1^w)^{2p}$  is symmetric, and the elements of  $(\mathbf{D}_1^w)^{2p}$  satisfy

$$[(\mathbf{D}_1^w)^{2p}]_{k,k+m} = [(\mathbf{D}_1^w)^{2p}]_{k,k-m}, \quad [(\mathbf{D}_1^w)^{2p}]_{k,m+N_w} = [(\mathbf{D}_1^w)^{2p}]_{k,m},$$

where  $k, m = 1, \dots, N_w$ .

2.  $(\mathbf{D}_1^w)^{2p-1}$  is skew-symmetric and the elements of  $(\mathbf{D}_1^w)^{2p-1}$  satisfy

$$\begin{aligned} [(\mathbf{D}_1^w)^{2p-1}]_{k,k+N_w/2} &= 0, \quad [(\mathbf{D}_1^w)^{2p-1}]_{k,k+m} = -[(\mathbf{D}_1^w)^{2p-1}]_{k,k-m}, \\ [(\mathbf{D}_1^w)^{2p-1}]_{k,m+N_w} &= [(\mathbf{D}_1^w)^{2p-1}]_{k,m}, \end{aligned}$$

where  $k, m = 1, \dots, N_w$ .

**Proof.** By noting the relationship (3.3) and Eq. (3.5), we finish the proof.  $\square$

**Lemma 3.3.** [19] For the matrix  $\mathbf{D}_p^w$ ,  $p = 1, 2, \dots$ , we have

$$\mathbf{D}_p^w = \begin{cases} \mathcal{F}_{N_w}^{-1} \mathbf{\Lambda}_w^p \mathcal{F}_{N_w}, & p \text{ is an odd integer,} \\ \mathcal{F}_{N_w}^{-1} \tilde{\mathbf{\Lambda}}_w^p \mathcal{F}_{N_w}, & p \text{ is an even integer,} \end{cases}$$

where  $\mathbf{\Lambda}_w$  and  $\tilde{\mathbf{\Lambda}}_w$  are the diagonal matrices whose (non-zero) entries are the scaled wave-numbers

$$\begin{aligned} \mathbf{\Lambda}_w &= i\mu_w \text{diag}(0, 1, \dots, \frac{N_w}{2} - 1, 0, -\frac{N_w}{2} + 1, \dots, -2, -1), \\ \tilde{\mathbf{\Lambda}}_w &= i\mu_w \text{diag}(0, 1, \dots, \frac{N_w}{2} - 1, \frac{N_w}{2}, -\frac{N_w}{2} + 1, \dots, -2, -1), \end{aligned}$$

and  $\mathcal{F}_{N_w}$  is the matrix of DFT coefficients with entries given by  $(\mathcal{F}_{N_w})_{j,k} = \omega_{N_w}^{-j,k}$ ,  $\omega_{N_w} = e^{i\frac{2\pi}{N_w}}$ ,  $(\mathcal{F}_{N_w}^{-1})_{j,k} = \frac{1}{N_w} \omega_{N_w}^{j,k}$ .

Next, applying the Fourier pseudo-spectral methods to the Hamiltonian formulation (2.3), we can obtain

$$\frac{d}{dt} \begin{pmatrix} \mathbf{H} \\ \mathbf{E} \end{pmatrix} = \begin{pmatrix} 0 & -\mathbf{I} \\ \mathbf{I} & 0 \end{pmatrix} \begin{pmatrix} \nabla_{\mathbf{H}} \bar{\mathcal{H}}_1 \\ \nabla_{\mathbf{E}} \bar{\mathcal{H}}_1 \end{pmatrix} = \begin{pmatrix} 0 & -\mathbf{I} \\ \mathbf{I} & 0 \end{pmatrix} \begin{pmatrix} \epsilon^{-1} \mathbf{D}\mathbf{H} \\ \mu^{-1} \mathbf{D}\mathbf{E} \end{pmatrix} = \hat{\mathcal{J}}_1 \nabla \bar{\mathcal{H}}_1, \quad (3.6)$$

where  $\mathbf{I} \in \mathbb{R}^{3s_1 \times 3s_1}$ ,  $s_1 = N_x \times N_y \times N_z$ ,

$$\bar{\mathcal{H}}_1 = \frac{1}{2\epsilon} \mathbf{H}^T (\mathbf{D}\mathbf{H}) + \frac{1}{2\mu} \mathbf{E}^T (\mathbf{D}\mathbf{E}), \quad (3.7)$$

and

$$\begin{aligned} \mathbf{D} &= \begin{pmatrix} 0 & -\mathbf{D}_1^z \otimes \mathbf{I}_{N_y} \otimes \mathbf{I}_{N_x} & \mathbf{I}_{N_x} \otimes \mathbf{D}_1^y \otimes \mathbf{I}_{N_x} \\ \mathbf{D}_1^z \otimes \mathbf{I}_{N_y} \otimes \mathbf{I}_{N_x} & 0 & -\mathbf{I}_{N_z} \otimes \mathbf{I}_{N_y} \otimes \mathbf{D}_1^x \\ -\mathbf{I}_{N_x} \otimes \mathbf{D}_1^y \otimes \mathbf{I}_{N_x} & \mathbf{I}_{N_z} \otimes \mathbf{I}_{N_y} \otimes \mathbf{D}_1^x & 0 \end{pmatrix} \\ &:= \begin{pmatrix} 0 & -\mathbf{D}_3 & \mathbf{D}_2 \\ \mathbf{D}_3 & 0 & -\mathbf{D}_1 \\ -\mathbf{D}_2 & \mathbf{D}_1 & 0 \end{pmatrix}, \end{aligned} \quad (3.8)$$

is symmetric structure matrix corresponding to the discretization of the operator  $\nabla \times$ .

**Remark 3.1.** The matrices  $\mathbf{D}_1$ ,  $\mathbf{D}_2$ , and  $\mathbf{D}_3$  admit the following properties

1. Commutative law of multiplication

$$\mathbf{D}_{s_2} \mathbf{D}_{s_3} = \mathbf{D}_{s_3} \mathbf{D}_{s_2},$$

where  $s_2, s_3 = 1, 2, 3$ , and  $s_2 \neq s_3$ .

2. Skew symmetry

$$\mathbf{D}_p^T = -\mathbf{D}_p, \quad p = 1, 2, 3.$$

Moreover, one should note that the components of  $\mathbf{H}$  and  $\mathbf{E}$  in Eqs. (3.6)-(3.7) are the values of grid functions and different from those in (2.1). Without being confused, the notations  $\mathbf{H}$  and  $\mathbf{E}$  are still be adopted in the subsequent sections.



### 3.2 Sixth order AVF method approximation in time

In this subsection, the sixth order average vector field (AVF) method [27] will be employed to discretize finite dimensional Hamiltonian system (3.6) in time. For ordinary differential equations (ODEs)

$$\frac{d\mathbf{y}}{dt} = f(\mathbf{y}), \quad \mathbf{y}(0) = \mathbf{y}_0 \in \mathbb{R}^{2d}, \quad (3.9)$$

the AVF method is defined by

$$\frac{\mathbf{y}^{n+1} - \mathbf{y}^n}{\tau} = \int_0^1 f((1 - \xi)\mathbf{y}^n + \xi\mathbf{y}^{n+1})d\xi, \quad (3.10)$$

where  $\tau$  is the time step. The average vector field (AVF) method (3.10), which was first derived in Ref. [32], and then identified as a B-series method in Ref. [37], is affine-covariant, of order 2 and self-adjoint [10]. The remarkable advantage of the AVF method (3.10) is that it can preserve exactly the energy integral for any Hamiltonian system with a constant structure matrix. With the help of the concrete formulas of the substitution law [11, 17] for the trees of order 5, the second order AVF method (3.10) was extended to sixth order for the Hamiltonian system with a constant structure matrix [27]. The sixth order AVF method can be rewritten as a compact form [27]

$$\frac{\mathbf{y}^{n+1} - \mathbf{y}^n}{\tau} = \tilde{\mathbf{S}}\left(\frac{\mathbf{y}^{n+1} + \mathbf{y}^n}{2}\right) \int_0^1 \nabla H((1 - \xi)\mathbf{y}^n + \xi\mathbf{y}^{n+1})d\xi, \quad (3.11)$$

where

$$\begin{aligned} \tilde{\mathbf{S}}(\mathbf{y}) = & \left[ \mathbf{I}_{2d \times 2d} - \frac{\tau^2}{12} \mathbf{S} \mathcal{H} \mathbf{S} \mathcal{H} + \frac{\tau^4}{720} \left( 6 \mathbf{S} \mathcal{H} \mathbf{S} \mathcal{H} \mathbf{S} \mathcal{H} \mathbf{S} \mathcal{H} - \mathbf{S} \mathcal{T} \mathbf{S} \mathcal{T} + \mathbf{S} \mathcal{H} \mathbf{S} \mathcal{H} \mathbf{S} \mathcal{T} \right. \right. \\ & \left. \left. - \mathbf{S} \mathcal{T} \mathbf{S} \mathcal{H} \mathbf{S} \mathcal{H} - \frac{3}{2} \mathbf{S} \mathcal{H} \mathbf{S} \mathcal{L} - \frac{3}{2} \mathbf{S} \mathcal{L} \mathbf{S} \mathcal{H} + 3 \mathbf{S} \mathcal{R} \mathbf{S} \mathcal{H} + 3 \mathbf{S} \mathcal{H} \mathbf{S} \mathcal{R} \right) \right] \mathbf{S}, \end{aligned}$$

$\mathbf{S}$  is the constant structure matrix,  $H(\mathbf{y}) : \mathbb{R}^{2d} \rightarrow \mathbb{R}$  is Hamiltonian function, and the symmetric matrices  $\mathcal{H}(\mathbf{y})$ ,  $\mathcal{T}(\mathbf{y})$ ,  $\mathcal{L}(\mathbf{y})$  and  $\mathcal{R}(\mathbf{y})$  are given by the Einstein summation convention

$$\begin{aligned} \mathcal{H}_{ij} & := \frac{\partial^2 H}{\partial y_i \partial y_j}, \quad \mathcal{T}_{ij} := \frac{\partial^3 H}{\partial y_i \partial y_j \partial y_k} S^{kl} \frac{\partial H}{\partial y_l}, \\ \mathcal{L}_{ij} & := \frac{\partial^4 H}{\partial y_i \partial y_j \partial y_k \partial y_l} S^{km} \frac{\partial H}{\partial y_m} S^{ln} \frac{\partial H}{\partial y_n}, \quad \mathcal{R}_{ij} := \frac{\partial^3 H}{\partial y_i \partial y_j \partial y_k} S^{kl} \frac{\partial^2 H}{\partial y_l \partial y_m} S^{mn} \frac{\partial H}{\partial y_n}. \end{aligned}$$

Some others works on the AVF method can be found in Refs. [9, 16].

Applying the sixth order AVF method (3.11) to Eq. (3.6), we can obtain

$$\begin{aligned} \frac{1}{\tau} \begin{pmatrix} \mathbf{H}^{n+1} - \mathbf{H}^n \\ \mathbf{E}^{n+1} - \mathbf{E}^n \end{pmatrix} = & \left[ \begin{pmatrix} \mathbf{I} & 0 \\ 0 & \mathbf{I} \end{pmatrix} - \frac{\tau^2}{12} \begin{pmatrix} -c^2 \mathbf{D}^2 & 0 \\ 0 & -c^2 \mathbf{D}^2 \end{pmatrix} - \frac{\tau^4}{120} \begin{pmatrix} -c^4 \mathbf{D}^4 & 0 \\ 0 & -c^4 \mathbf{D}^4 \end{pmatrix} \right] \\ & \begin{pmatrix} 0 & -\mathbf{I} \\ \mathbf{I} & 0 \end{pmatrix} \begin{pmatrix} \varepsilon^{-1} \mathbf{D} \int_0^1 ((1 - \xi)\mathbf{H}^n + \xi\mathbf{H}^{n+1})d\xi \\ \mu^{-1} \mathbf{D} \int_0^1 ((1 - \xi)\mathbf{E}^n + \xi\mathbf{E}^{n+1})d\xi \end{pmatrix}, \quad (3.12) \end{aligned}$$

where  $c = 1/\sqrt{\varepsilon\mu}$ . The integration in Eq. (3.12) can be calculated exactly to give

$$\frac{1}{\tau} \begin{pmatrix} \mathbf{H}^{n+1} - \mathbf{H}^n \\ \mathbf{E}^{n+1} - \mathbf{E}^n \end{pmatrix} = \left[ \begin{pmatrix} 0 & -\mathbf{D} \\ \mathbf{D} & 0 \end{pmatrix} + \frac{c^2 \tau^2}{12} \begin{pmatrix} 0 & -\mathbf{D}^3 \\ \mathbf{D}^3 & 0 \end{pmatrix} + \frac{c^4 \tau^4}{120} \begin{pmatrix} 0 & -\mathbf{D}^5 \\ \mathbf{D}^5 & 0 \end{pmatrix} \right]$$

$$\begin{pmatrix} \varepsilon^{-1}(\mathbf{H}^{n+1} + \mathbf{H}^n)/2 \\ \mu^{-1}(\mathbf{E}^{n+1} + \mathbf{E}^n)/2 \end{pmatrix}, \quad (3.13)$$

which comprises our sixth order energy-conserved scheme for the 3D Maxwell's equations. In fact, Eqs. (3.13) can be expressed as an equivalent form

$$\begin{pmatrix} \frac{2\mu}{\tau}\mathbf{I} & \hat{\mathbf{D}} \\ -\hat{\mathbf{D}} & \frac{2\varepsilon}{\tau}\mathbf{I} \end{pmatrix} \begin{pmatrix} \mathbf{H}^{n+1} \\ \mathbf{E}^{n+1} \end{pmatrix} = \begin{pmatrix} \frac{2\mu}{\tau}\mathbf{I} & -\hat{\mathbf{D}} \\ \hat{\mathbf{D}} & \frac{2\varepsilon}{\tau}\mathbf{I} \end{pmatrix} \begin{pmatrix} \mathbf{H}^n \\ \mathbf{E}^n \end{pmatrix}, \quad (3.14)$$

where  $\hat{\mathbf{D}} = \mathbf{D} + \frac{c^2\tau^2}{12}\mathbf{D}^3 + \frac{c^4\tau^4}{120}\mathbf{D}^5$ .

**Remark 3.2.** *If exchanging  $n + 1 \leftrightarrow n$  and  $\tau \leftrightarrow -\tau$ , then we find that the scheme (3.13) unaltered. Thus, according to Ref. [20], the scheme (3.13) is symmetric. Moreover, the proposed scheme is uniquely solvable (see Appendix).*

## 4 Discrete conservation laws and divergence preservation

In this section, we will rigorously prove the scheme (3.13) satisfies the discrete version of the five energy conservation laws, the three momentum conservation laws, the symplecticity as well as the two discrete divergence-free fields. But before, we introduce a new semi-norm for any grid functions  $U_{j,k,m}, (x_j, y_k, z_m) \in \Omega_h$ ,

$$\|U\|_{D_1^x, h} = \langle D_1 U, D_1 U \rangle_h^{\frac{1}{2}}, \quad \|U\|_{D_1^y, h} = \langle D_2 U, D_2 U \rangle_h^{\frac{1}{2}}, \quad \|U\|_{D_1^z, h} = \langle D_3 U, D_3 U \rangle_h^{\frac{1}{2}},$$

and

$$\|U\|_{D_1^w, h}^2 = \|U_x\|_{D_1^w, h}^2 + \|U_y\|_{D_1^w, h}^2 + \|U_z\|_{D_1^w, h}^2,$$

for a vector  $U = [(U_x)^T, (U_y)^T, (U_z)^T]^T$ .

**Theorem 4.1.** *The solutions  $\mathbf{H}^n$  and  $\mathbf{E}^n$  of the proposed scheme (3.13) satisfy the discrete symplectic conservation law*

$$\omega^{n+1} = \omega^n, \quad \omega^n = d\mathbf{E}^n \wedge d\mathbf{H}^n, \quad n = 0, \dots, M-1, \quad (4.1)$$

where

$$\begin{aligned} d\mathbf{E}^n \wedge d\mathbf{H}^n &= d\mathbf{E}_x^n \wedge d\mathbf{H}_x^n + d\mathbf{E}_y^n \wedge d\mathbf{H}_y^n + d\mathbf{E}_z^n \wedge d\mathbf{H}_z^n, \\ d\mathbf{E}_w^n \wedge d\mathbf{H}_w^n &= \sum_{j,k,m} d\mathbf{E}_{w,j,k,m}^n \wedge d\mathbf{H}_{w,j,k,m}^n. \end{aligned}$$

**Proof.** Eq. (3.13) can be rewritten as

$$\begin{pmatrix} 0 & I \\ -I & 0 \end{pmatrix} \begin{pmatrix} \frac{\mathbf{H}^{n+1} - \mathbf{H}^n}{\tau} \\ \frac{\mathbf{E}^{n+1} - \mathbf{E}^n}{\tau} \end{pmatrix} = \begin{pmatrix} \varepsilon^{-1}\hat{\mathbf{D}} & 0 \\ 0 & \mu^{-1}\hat{\mathbf{D}} \end{pmatrix} \begin{pmatrix} \frac{\mathbf{H}^{n+1} + \mathbf{H}^n}{2} \\ \frac{\mathbf{E}^{n+1} + \mathbf{E}^n}{2} \end{pmatrix}. \quad (4.2)$$

The variational equations associated with Eq. (4.2) read

$$\begin{pmatrix} 0 & I \\ -I & 0 \end{pmatrix} \begin{pmatrix} \frac{d\mathbf{H}^{n+1} - d\mathbf{H}^n}{\tau} \\ \frac{d\mathbf{E}^{n+1} - d\mathbf{E}^n}{\tau} \end{pmatrix} = \begin{pmatrix} \varepsilon^{-1}\hat{\mathbf{D}} & 0 \\ 0 & \mu^{-1}\hat{\mathbf{D}} \end{pmatrix} \begin{pmatrix} \frac{d\mathbf{H}^{n+1} + d\mathbf{H}^n}{2} \\ \frac{d\mathbf{E}^{n+1} + d\mathbf{E}^n}{2} \end{pmatrix}. \quad (4.3)$$

Taking the wedge product with  $\begin{pmatrix} \frac{d\mathbf{H}^{n+1} + d\mathbf{H}^n}{2} \\ \frac{d\mathbf{E}^{n+1} + d\mathbf{E}^n}{2} \end{pmatrix}$  on both sides of Eq. (4.3) and noting the fact

$$\begin{pmatrix} \frac{d\mathbf{H}^{n+1} + d\mathbf{H}^n}{2} \\ \frac{d\mathbf{E}^{n+1} + d\mathbf{E}^n}{2} \end{pmatrix} \wedge \begin{pmatrix} \varepsilon^{-1}\hat{\mathbf{D}} & 0 \\ 0 & \mu^{-1}\hat{\mathbf{D}} \end{pmatrix} \begin{pmatrix} \frac{d\mathbf{H}^{n+1} + d\mathbf{H}^n}{2} \\ \frac{d\mathbf{E}^{n+1} + d\mathbf{E}^n}{2} \end{pmatrix} = 0, \quad (4.4)$$

we obtain the discrete symplectic conservation law (4.1).  $\square$

**Remark 4.1.** Since the system of the Maxwell's equations (2.1) is linear, we can get the symplectic conservation law for the method (3.13). Usually, energy-conserved methods do not imply the preservation of the symplectic conservation law for the given system.

Since the AVF method can preserve Hamiltonian energy automatically, we can derive the following energy conservation laws, immediately.

**Theorem 4.2.** The solutions  $\mathbf{H}^n$  and  $\mathbf{E}^n$  of the proposed scheme (3.13) satisfy the discrete energy conservation laws

$$\mathcal{E}_1^{n+1} = \mathcal{E}_1^n, \quad \mathcal{E}_1^n = \frac{1}{2\epsilon} \langle \mathbf{H}^n, \mathbf{D}\mathbf{H}^n \rangle_h + \frac{1}{2\mu} \langle \mathbf{E}^n, \mathbf{D}\mathbf{E}^n \rangle_h, \quad n = 0, \dots, M-1, \quad (4.5)$$

and

$$\mathcal{E}_2^{n+1} = \mathcal{E}_2^n, \quad \mathcal{E}_2^n = \frac{\mu}{2} \|\mathbf{H}^n\|_h^2 + \frac{\epsilon}{2} \|\mathbf{E}^n\|_h^2, \quad n = 0, \dots, M-1. \quad (4.6)$$

In addition, the scheme (3.13) also satisfies the following energy conservation laws.

**Theorem 4.3.** The solutions  $\mathbf{H}^n$  and  $\mathbf{E}^n$  of the scheme (3.13) satisfy the discrete energy conservation law

$$\mathcal{E}_3^{n+1} = \mathcal{E}_3^n, \quad \mathcal{E}_3^n = \frac{\mu}{2} \|\hat{\delta}_t \mathbf{H}^{n-1/2}\|_h^2 + \frac{\epsilon}{2} \|\hat{\delta}_t \mathbf{E}^{n-1/2}\|_h^2, \quad n = 1, \dots, M-1. \quad (4.7)$$

**Proof.** We can deduce from (3.13)

$$\frac{1}{\tau} \begin{pmatrix} \mu \hat{\delta}_t \mathbf{H}^{n+1/2} - \mu \hat{\delta}_t \mathbf{H}^{n-1/2} \\ \epsilon \hat{\delta}_t \mathbf{E}^{n+1/2} - \epsilon \hat{\delta}_t \mathbf{E}^{n-1/2} \end{pmatrix} = \begin{pmatrix} 0 & -\hat{\mathbf{D}} \\ \hat{\mathbf{D}} & 0 \end{pmatrix} \begin{pmatrix} \frac{1}{2} (\hat{\delta}_t \mathbf{H}^{n+1/2} + \hat{\delta}_t \mathbf{H}^{n-1/2}) \\ \frac{1}{2} (\hat{\delta}_t \mathbf{E}^{n+1/2} + \hat{\delta}_t \mathbf{E}^{n-1/2}) \end{pmatrix}. \quad (4.8)$$

Making the inner product with  $\frac{1}{2} \begin{pmatrix} \hat{\delta}_t \mathbf{H}^{n+1/2} + \hat{\delta}_t \mathbf{H}^{n-1/2} \\ \hat{\delta}_t \mathbf{E}^{n+1/2} + \hat{\delta}_t \mathbf{E}^{n-1/2} \end{pmatrix}$  on both sides of Eq. (4.8)

and by virtue of the skew-symmetric property of the matrix  $\begin{pmatrix} 0 & -\hat{\mathbf{D}} \\ \hat{\mathbf{D}} & 0 \end{pmatrix}$ , we finish the proof.  $\square$

**Theorem 4.4.** The solutions  $\mathbf{H}^n$  and  $\mathbf{E}^n$  of the proposed scheme (3.13) also possess the discrete energy conservation laws

$$\mathcal{E}_{4w}^{n+1} = \mathcal{E}_{4w}^n, \quad \mathcal{E}_{4w}^n = \mu \|\mathbf{H}^n\|_{\mathbf{D}_1^w, h}^2 + \epsilon \|\mathbf{E}^n\|_{\mathbf{D}_1^w, h}^2, \quad n = 0, \dots, M-1, \quad (4.9)$$

and

$$\mathcal{E}_{5w}^{n+1} = \mathcal{E}_{5w}^n, \quad \mathcal{E}_{5w}^n = \mu \|\hat{\delta}_t \mathbf{H}^{n-1/2}\|_{\mathbf{D}_1^w, h}^2 + \epsilon \|\hat{\delta}_t \mathbf{E}^{n-1/2}\|_{\mathbf{D}_1^w, h}^2, \quad n = 1, \dots, M-1. \quad (4.10)$$

**Proof.** We define block diagonal matrices  $\mathbf{M}_x = \begin{pmatrix} \mathbf{D}_1 & & \\ & \mathbf{D}_1 & \\ & & \mathbf{D}_1 \end{pmatrix}$ ,  $\mathbf{M}_y = \begin{pmatrix} \mathbf{D}_2 & & \\ & \mathbf{D}_2 & \\ & & \mathbf{D}_2 \end{pmatrix}$ , and  $\mathbf{M}_z = \begin{pmatrix} \mathbf{D}_3 & & \\ & \mathbf{D}_3 & \\ & & \mathbf{D}_3 \end{pmatrix}$ . According to Remark 3.1, it is easy to see that  $\mathbf{M}_w \hat{\mathbf{D}} =$

$\hat{D}\mathbf{M}_w$ . Then, left-multiplying (3.13) with block diagonal matrix  $\mathbf{G}_w = \begin{pmatrix} \mathbf{M}_w & \\ & \mathbf{M}_w \end{pmatrix}$ , we have

$$\frac{1}{\tau} \begin{pmatrix} \mu(\mathbf{M}_w \mathbf{H}^{n+1}) - \mu(\mathbf{M}_w \mathbf{H}^n) \\ \epsilon(\mathbf{M}_w \mathbf{E}^{n+1}) - \epsilon(\mathbf{M}_w \mathbf{E}^n) \end{pmatrix} = \begin{pmatrix} 0 & -\hat{D} \\ \hat{D} & 0 \end{pmatrix} \begin{pmatrix} \frac{\mathbf{M}_w \mathbf{H}^{n+1} + \mathbf{M}_w \mathbf{H}^n}{2} \\ \frac{\mathbf{M}_w \mathbf{E}^{n+1} + \mathbf{M}_w \mathbf{E}^n}{2} \end{pmatrix}. \quad (4.11)$$

Computing the inner product with  $\begin{pmatrix} \mathbf{M}_w \mathbf{H}^{n+1} + \mathbf{M}_w \mathbf{H}^n \\ \mathbf{M}_w \mathbf{E}^{n+1} + \mathbf{M}_w \mathbf{E}^n \end{pmatrix}$  on both sides of Eq. (4.11) and we can derive that

$$\mu \|\mathbf{M}_w \mathbf{H}^{n+1}\|^2 + \epsilon \|\mathbf{M}_w \mathbf{E}^{n+1}\|_h^2 = \mu \|\mathbf{M}_w \mathbf{H}^n\|^2 + \epsilon \|\mathbf{M}_w \mathbf{E}^n\|_h^2. \quad (4.12)$$

Note the notation introduced for grid vector function and we can get the discrete energy conservation law (4.9).  $\square$

Left-multiplying (4.8) with the block diagonal matrix  $\mathbf{G}_w$ , and taking the inner product with

$$\begin{pmatrix} \hat{\delta}_t \mathbf{M}_w \mathbf{H}^{n+1/2} + \hat{\delta}_t \mathbf{M}_w \mathbf{H}^{n-1/2} \\ \hat{\delta}_t \mathbf{M}_w \mathbf{E}^{n+1/2} + \hat{\delta}_t \mathbf{M}_w \mathbf{E}^{n-1/2} \end{pmatrix},$$

we can obtain the second discrete energy conservation law of Theorem 4.4.

Next, we can show that the resulting numerical scheme (3.13) preserves the corresponding discrete momentum conservation laws.

**Theorem 4.5.** *The solutions  $\mathbf{H}^n$  and  $\mathbf{E}^n$  of the proposed scheme (3.13) capture momentum conservation laws*

$$\mathcal{M}_w^{n+1} = \mathcal{M}_w^n, \quad \mathcal{M}_w^n = \langle \mathbf{H}^n, \mathbf{M}_w \mathbf{E}^n \rangle_h, \quad n = 0, \dots, M-1, \quad (4.13)$$

where  $\mathbf{M}_w$  is defined as above.

**Proof.** Eq. (4.11) can be rewritten as

$$\frac{1}{\tau} \begin{pmatrix} \mathbf{M}_w \mathbf{H}^{n+1} - \mathbf{M}_w \mathbf{H}^n \\ -(\mathbf{M}_w \mathbf{E}^{n+1} - \mathbf{M}_w \mathbf{E}^n) \end{pmatrix} = \begin{pmatrix} \mu^{-1} \hat{D} \mathbf{M}_w \mathbf{E}^{n+1/2} \\ \epsilon^{-1} \hat{D} \mathbf{M}_w \mathbf{H}^{n+1/2} \end{pmatrix}. \quad (4.14)$$

Then taking the inner product with  $\begin{pmatrix} \mathbf{E}^{n+1/2} \\ \mathbf{H}^{n+1/2} \end{pmatrix}$  on both sides of Eq. (4.14) and we have

$$\begin{aligned} \frac{1}{\tau} \left( \langle \mathbf{H}^{n+1}, \mathbf{M}_w \mathbf{E}^{n+1} \rangle - \langle \mathbf{H}^n, \mathbf{M}_w \mathbf{E}^n \rangle_h \right) &= -\mu^{-1} \langle \mathbf{E}^{n+1/2}, \hat{D} \mathbf{M}_w \mathbf{E}^{n+1/2} \rangle_h \\ &\quad - \epsilon^{-1} \langle \mathbf{H}^{n+1/2}, \hat{D} \mathbf{M}_w \mathbf{H}^{n+1/2} \rangle_h. \end{aligned} \quad (4.15)$$

By noting  $(\hat{D} \mathbf{M}_w)^T = -\hat{D} \mathbf{M}_w$ , we can obtain (4.13).  $\square$

Finally, we show that the proposed scheme (3.13) can preserve the two discrete divergence-free fields of the Maxwell's equations.

**Theorem 4.6.** *For the scheme (3.13), the following discrete divergence-free fields hold*

$$\bar{\nabla} \cdot (\epsilon \mathbf{E}^{n+1}) = \bar{\nabla} \cdot (\epsilon \mathbf{E}^n) \quad \text{and} \quad \bar{\nabla} \cdot (\mu \mathbf{H}^{n+1}) = \bar{\nabla} \cdot (\mu \mathbf{H}^n), \quad n = 0, \dots, M-1, \quad (4.16)$$

where  $\bar{\nabla} = \begin{pmatrix} D_1 \\ D_2 \\ D_3 \end{pmatrix}$ , corresponding to the discretization of the operator  $\nabla$  and

$$\begin{aligned}\bar{\nabla} \cdot (\mu \mathbf{H}) &= D_1(\mu \mathbf{H}_x) + D_2(\mu \mathbf{H}_y) + D_3(\mu \mathbf{H}_z), \\ \bar{\nabla} \cdot (\epsilon \mathbf{E}) &= D_1(\epsilon \mathbf{E}_x) + D_2(\epsilon \mathbf{E}_y) + D_3(\epsilon \mathbf{E}_z).\end{aligned}$$

**Proof.** Eq. (3.13) is equivalent to

$$\frac{\mu \mathbf{H}^{n+1} - \mu \mathbf{H}^n}{\tau} = -\hat{D} \frac{\mathbf{E}^{n+1} + \mathbf{E}^n}{2}, \quad (4.17)$$

$$\frac{\epsilon \mathbf{E}^{n+1} - \epsilon \mathbf{E}^n}{\tau} = \hat{D} \frac{\mathbf{H}^{n+1} + \mathbf{H}^n}{2}. \quad (4.18)$$

Left-multiplying (4.17) and (4.18) with  $\bar{\nabla} \cdot$ , we then can have

$$\frac{\bar{\nabla} \cdot (\mu \mathbf{H}^{n+1}) - \bar{\nabla} \cdot (\mu \mathbf{H}^n)}{\tau} = -\bar{\nabla} \cdot \left( \hat{D} \frac{\mathbf{E}^{n+1} + \mathbf{E}^n}{2} \right), \quad (4.19)$$

$$\frac{\bar{\nabla} \cdot (\epsilon \mathbf{E}^{n+1}) - \bar{\nabla} \cdot (\epsilon \mathbf{E}^n)}{\tau} = \bar{\nabla} \cdot \left( \hat{D} \frac{\mathbf{H}^{n+1} + \mathbf{H}^n}{2} \right), \quad (4.20)$$

whilst the right terms are equal to zero by careful calculation. This completes the proof.  $\square$

**Remark 4.2.** Eqs. (4.16) are not, strictly speaking, divergence-free, as  $\bar{\nabla} \cdot (\epsilon \mathbf{E}^0) \neq \mathbf{0}$  and  $\bar{\nabla} \cdot (\epsilon \mathbf{H}^0) \neq \mathbf{0}$ . However,  $\bar{\nabla}$  is a higher approximation to  $\nabla$  in space, so, by choosing appropriate collocation points,  $\|\bar{\nabla} \cdot (\epsilon \mathbf{E}^0)\|_{h,\infty}$  and  $\|\bar{\nabla} \cdot (\epsilon \mathbf{H}^0)\|_{h,\infty}$  can reach machine precision in practical computation (see Ref. [6] and Section 7). Thus, we also refer to Eqs. (4.16) as divergence free.

## 5 Convergence analysis

In this section, we will establish error estimate of the proposed scheme (3.13). For simplicity, we let  $\Omega = [0, 2\pi]^3$ ,  $L^2(\Omega)$  with the inner product  $\langle \cdot, \cdot \rangle$  and the norm  $\|\cdot\|$  defined previously. For any positive integer  $r$ , the semi-norm and the norm of  $H^r(\Omega)$  are denoted by  $|\cdot|_r$  and  $\|\cdot\|_r$ , respectively.  $\|\cdot\|_0$  is denoted by  $\|\cdot\|$  for simplicity. Let  $C_p^\infty$  be the set of infinitely differentiable functions with period  $2\pi$  defined on  $\Omega$  for all variables.  $H_p^r(\Omega)$  is the closure of  $C_p^\infty$  in  $H^r(\Omega)$ .

let  $N_x = N_y = N_z = N$ , the interpolation space  $S_N'''$  can be written as

$$\begin{aligned}S_N''' = \left\{ u \mid u = \sum_{|j|,|k|,|m| \leq \frac{N}{2}} \frac{\hat{u}_{j,k,m}}{c_j c_k c_m} e^{i(jx+ky+mz)} : \hat{u}_{\frac{N}{2},k,m} = \hat{u}_{-\frac{N}{2},k,m}, \right. \\ \left. \hat{u}_{j,\frac{N}{2},m} = \hat{u}_{j,-\frac{N}{2},m}, \hat{u}_{j,k,\frac{N}{2}} = \hat{u}_{j,k,-\frac{N}{2}} \right\},\end{aligned}$$

where  $c_l = 1$ ,  $|l| < \frac{N}{2}$ ,  $c_{-\frac{N}{2}} = c_{\frac{N}{2}} = 2$ .

We denote

$$S_N = \left\{ u \mid u = \sum_{|j|,|k|,|m| \leq \frac{N}{2}} \hat{u}_{j,k,m} e^{i(jx+ky+mz)} \right\}. \quad (5.1)$$

It is remarked that  $S_N''' \subseteq S_N$  and  $S_{N-2} \subseteq S_N'''$ . We denote  $P_N : [L^2(\Omega)]^3 \rightarrow [S_N]^3$  as the orthogonal projection operator and recall the interpolation operator  $I_N : [C(\Omega)]^3 \rightarrow [S_N''' ]^3$ . By noting  $P_N \partial_w u = \partial_w P_N u$ ,  $w = x, y, z$ , we can see that  $\nabla \times$  and  $P_N$  satisfy the commutative law.

**Lemma 5.1.** [6] For  $\mathbf{u} \in [S_N''']^3$ ,  $\|\mathbf{u}\| \leq \|\mathbf{u}\|_h \leq 2\sqrt{2}\|\mathbf{u}\|$ .

**Lemma 5.2.** [8] If  $0 \leq \alpha \leq r$  and  $\mathbf{u} \in [H_p^r(\Omega)]^3$ , then

$$\|P_N \mathbf{u} - \mathbf{u}\|_\alpha \leq CN^{\alpha-r} |\mathbf{u}|_r, \quad (5.2)$$

and in addition if  $r > \frac{3}{2}$  then

$$\|I_N \mathbf{u} - \mathbf{u}\|_\alpha \leq CN^{\alpha-r} |\mathbf{u}|_r. \quad (5.3)$$

**Lemma 5.3.** If  $\mathbf{u}^* = P_{N-2} \mathbf{u}$ ,  $\mathbf{u} \in [H_p^r(\Omega)]^3$ ,  $N > 2$ ,  $r > \frac{3}{2}$ , then  $\|\mathbf{u}^* - \mathbf{u}\|_N \leq CN^{-r} |\mathbf{u}|_r$ .

**Proof.** By virtue of Lemmas 5.1 and 5.2, we have

$$\begin{aligned} \|\mathbf{u} - \mathbf{u}^*\|_h &= \|I_N(\mathbf{u} - \mathbf{u}^*)\|_h \\ &\leq 2\sqrt{2} \|I_N(\mathbf{u} - \mathbf{u}^*)\| = 2\sqrt{2} \|I_N \mathbf{u} - \mathbf{u}^*\| \\ &\leq 2\sqrt{2} (\|I_N \mathbf{u} - \mathbf{u}\| + \|\mathbf{u} - \mathbf{u}^*\|) \leq CN^{-r} |\mathbf{u}|_r. \end{aligned}$$

**Theorem 5.1.** Suppose that the exact periodic solution components  $\mathbf{H}$  and  $\mathbf{E}$  are smooth enough:  $\mathbf{H}, \mathbf{E} \in C^7(0, T; [H_p^r(\Omega)]^3)$ ,  $r > \frac{10}{2}$ . The initial conditions are  $\mathbf{H}_0, \mathbf{E}_0 \in ([H_p^r(\Omega)]^3)$ ,  $r > \frac{10}{2}$ . For  $n \geq 0$ , let  $\mathbf{H}^n$  and  $\mathbf{E}^n$  be the solutions of the scheme (3.13). Then, for any fixed  $T > 0$ , there exists a positive constant  $C$  independent of  $\tau, h_x, h_y$ , and  $h_z$ , which may be vary in different cases, such that

$$\max_{0 \leq n \leq M} (\epsilon \|\mathbf{H}(t_n) - \mathbf{H}^n\|_h^2 + \mu \|\mathbf{E}(t_n) - \mathbf{E}^n\|_h^2)^{\frac{1}{2}} \leq CT(\tau^6 + N^{-r}). \quad (5.4)$$

**Proof.** Let

$$\mathbf{E}^* = P_{N-2} \mathbf{E}, \quad \mathbf{H}^* = P_{N-2} \mathbf{H}.$$

The projection of Eqs. (2.1) are written as

$$\mu \partial_t \mathbf{H}^* + \nabla \times \mathbf{E}^* = 0, \quad \epsilon \partial_t \mathbf{E}^* - \nabla \times \mathbf{H}^* = 0. \quad (5.5)$$

Let

$$\Phi^{n+\frac{1}{2}} = \mu \delta_t (\mathbf{H}^*)^n + \nabla \times (\mathbf{E}^*)^{n+\frac{1}{2}} + \frac{c^2 \tau^2}{12} (\nabla \times)^3 (\mathbf{E}^*)^{n+\frac{1}{2}} + \frac{c^4 \tau^4}{120} (\nabla \times)^5 (\mathbf{E}^*)^{n+\frac{1}{2}}, \quad (5.6)$$

$$\Psi^{n+\frac{1}{2}} = \epsilon \delta_t (\mathbf{E}^*)^n - \nabla \times (\mathbf{H}^*)^{n+\frac{1}{2}} - \frac{c^2 \tau^2}{12} (\nabla \times)^3 (\mathbf{H}^*)^{n+\frac{1}{2}} - \frac{c^4 \tau^4}{120} (\nabla \times)^5 (\mathbf{H}^*)^{n+\frac{1}{2}}, \quad (5.7)$$

where  $n = 0, \dots, M-1$ . Eq. (5.6) can rewritten as

$$\Phi^{n+\frac{1}{2}} = \Phi_1^{n+\frac{1}{2}} + \Phi_2^{n+\frac{1}{2}}, \quad (5.8)$$

where

$$\begin{aligned} \Phi_1^{n+\frac{1}{2}} &= \mu \delta_t (\mathbf{H}^* - \mathbf{H})^n + \nabla \times (\mathbf{E}^* - \mathbf{E})^{n+\frac{1}{2}} + \frac{c^2 \tau^2}{12} (\nabla \times)^3 (\mathbf{E}^* - \mathbf{E})^{n+\frac{1}{2}} \\ &\quad + \frac{c^4 \tau^4}{120} (\nabla \times)^5 (\mathbf{E}^* - \mathbf{E})^{n+\frac{1}{2}}, \end{aligned}$$

and

$$\Phi_2^{n+\frac{1}{2}} = \mu\delta_t \mathbf{H}^n + \nabla \times \mathbf{E}^{n+\frac{1}{2}} + \frac{c^2\tau^2}{12}(\nabla \times)^3 \mathbf{E}^{n+\frac{1}{2}} + \frac{c^4\tau^4}{120}(\nabla \times)^5 \mathbf{E}^{n+\frac{1}{2}},$$

By using lemma 5.2 and Taylor's expansion at the node  $t_{n+\frac{1}{2}}$ , we can obtain

$$\|\Phi_1^{n+\frac{1}{2}}\| \leq C(\tau^6 + N^{-r}), \quad \|\Phi_2^{n+\frac{1}{2}}\| \leq C\tau^6, \quad n = 0, \dots, M-1. \quad (5.9)$$

Thus, we have

$$\|\Phi^{n+\frac{1}{2}}\| \leq C(\tau^6 + N^{-r}), \quad n = 0, \dots, M-1. \quad (5.10)$$

By noting  $\Phi^{n+\frac{1}{2}} \in [S_N''']^3$ , then, we can deduce from Lemma 5.1 that

$$\|\Phi^{n+\frac{1}{2}}\|_h \leq C(\tau^6 + N^{-r}), \quad n = 0, \dots, M-1. \quad (5.11)$$

By the analogous argument to  $\Phi^{n+\frac{1}{2}}$ , we have

$$\|\Psi^{n+\frac{1}{2}}\|_h \leq C(\tau^6 + N^{-r}), \quad n = 0, \dots, M-1. \quad (5.12)$$

Thus, from Eqs. (5.11) and (5.12), we have

$$(\|\Phi^{n+\frac{1}{2}}\|_h^2 + \|\Psi^{n+\frac{1}{2}}\|_h^2)^{\frac{1}{2}} \leq C(\tau^6 + N^{-r}), \quad n = 0, \dots, M-1, \quad (5.13)$$

where the inequation  $\sqrt{a^2 + b^2} \leq a + b, \forall a, b \geq 0$  is used.

Note that if  $\mathbf{E}^*, \mathbf{H}^* \in S_N'''$ , we can see that

$$\begin{aligned} \partial_x \tilde{U}^*(x_j, y_k, z_m) &= \partial_x I_N \tilde{U}^*(x_j, y_k, z_m) = [D_1 \tilde{U}^*]_{N_x N_y (m-1) + N_x (k-1) + j}, \\ \partial_y \tilde{U}^*(x_j, y_k, z_m) &= \partial_y I_N \tilde{U}^*(x_j, y_k, z_m) = [D_2 \tilde{U}^*]_{N_x N_y (m-1) + N_x (k-1) + j}, \\ \partial_z \tilde{U}^*(x_j, y_k, z_m) &= \partial_z I_N \tilde{U}^*(x_j, y_k, z_m) = [D_3 \tilde{U}^*]_{N_x N_y (m-1) + N_x (k-1) + j}, \end{aligned}$$

where

$$\tilde{U}^* = (U_{1,1,1}^*, \dots, U_{N_x,1,1}^*, U_{1,2,1}^*, \dots, U_{N_x,2,1}^*, \dots, U_{1,N_y,N_z}^*, \dots, U_{N_x,N_y,N_z}^*)^T.$$

By noting  $\mathbf{E}^*, \mathbf{H}^* \in S_N'''$ , we can get

$$\Phi^{n+\frac{1}{2}} = \mu\delta_t (\mathbf{H}^*)^n + \mathbf{D}(\mathbf{E}^*)^{n+\frac{1}{2}} + \frac{c^2\tau^2}{12} \mathbf{D}^3 (\mathbf{E}^*)^{n+\frac{1}{2}} + \frac{c^4\tau^4}{120} \mathbf{D}^5 (\mathbf{E}^*)^{n+\frac{1}{2}}, \quad (5.14)$$

$$\Psi^{n+\frac{1}{2}} = \epsilon\delta_t (\mathbf{E}^*)^n - \mathbf{D}(\mathbf{H}^*)^{n+\frac{1}{2}} - \frac{c^2\tau^2}{12} \mathbf{D}^3 (\mathbf{H}^*)^{n+\frac{1}{2}} - \frac{c^4\tau^4}{120} \mathbf{D}^5 (\mathbf{H}^*)^{n+\frac{1}{2}}, \quad (5.15)$$

where the components of the above vectors are the values of grid functions.

The scheme (3.13) can be rewritten as

$$\mu\delta_t \mathbf{H}^n + \mathbf{D}\mathbf{E}^{n+\frac{1}{2}} + \frac{c^2\tau^2}{12} \mathbf{D}^3 \mathbf{E}^{n+\frac{1}{2}} + \frac{c^4\tau^4}{120} \mathbf{D}^5 \mathbf{E}^{n+\frac{1}{2}} = 0, \quad (5.16)$$

$$\epsilon\delta_t \mathbf{E}^n - \mathbf{D}\mathbf{H}^{n+\frac{1}{2}} - \frac{c^2\tau^2}{12} \mathbf{D}^3 \mathbf{H}^{n+\frac{1}{2}} - \frac{c^4\tau^4}{120} \mathbf{D}^5 \mathbf{H}^{n+\frac{1}{2}} = 0. \quad (5.17)$$

Let  $\mathcal{H} = \mathbf{H}^* - \mathbf{H}$  and  $\mathcal{E} = \mathbf{E}^* - \mathbf{E}$ . Subtracting Eqs. (5.14)-(5.15) from Eqs. (5.16)-(5.17), respectively, we can obtain the error equations as follows

$$\mu\delta_t \mathcal{H}^n + \mathbf{D}\mathcal{E}^n + \frac{c^2\tau^2}{12} \mathbf{D}^3 \mathcal{E}^{n+\frac{1}{2}} + \frac{c^4\tau^4}{120} \mathbf{D}^5 \mathcal{E}^{n+\frac{1}{2}} = \Phi^{n+\frac{1}{2}}, \quad (5.18)$$

$$\epsilon \delta_t \mathcal{E}^n - \mathbf{D} \mathcal{H}^{n+\frac{1}{2}} - \frac{c^2 \tau^2}{12} \mathbf{D}^3 \mathcal{H}^{n+\frac{1}{2}} - \frac{c^4 \tau^4}{120} \mathbf{D}^5 \mathcal{H}^{n+\frac{1}{2}} = \Psi^{n+\frac{1}{2}}. \quad (5.19)$$

Computing the inner product of (5.18) and (5.19) with  $\mathcal{H}^{n+\frac{1}{2}}$  and  $\mathcal{E}^{n+\frac{1}{2}}$ , respectively, we can have

$$\begin{aligned} \langle \mu \delta_t \mathcal{H}^n, \mathcal{H}^{n+\frac{1}{2}} \rangle_h + \langle \mathbf{D} \mathcal{E}^{n+\frac{1}{2}}, \mathcal{H}^{n+\frac{1}{2}} \rangle_h + \frac{c^2 \tau^2}{12} \langle \mathbf{D}^3 \mathcal{E}^{n+\frac{1}{2}}, \mathcal{H}^{n+\frac{1}{2}} \rangle_h \\ + \frac{c^4 \tau^4}{120} \langle \mathbf{D}^5 \mathcal{E}^{n+\frac{1}{2}}, \mathcal{H}^{n+\frac{1}{2}} \rangle_h = \langle \Phi^{n+\frac{1}{2}}, \mathcal{H}^{n+\frac{1}{2}} \rangle_h, \end{aligned} \quad (5.20)$$

$$\begin{aligned} \langle \epsilon \delta_t \mathcal{E}^n, \mathcal{E}^{n+\frac{1}{2}} \rangle_h - \langle \mathbf{D} \mathcal{H}^{n+\frac{1}{2}}, \mathcal{E}^{n+\frac{1}{2}} \rangle_h - \frac{c^2 \tau^2}{12} \langle \mathbf{D}^3 \mathcal{H}^{n+\frac{1}{2}}, \mathcal{E}^{n+\frac{1}{2}} \rangle_h \\ - \frac{c^4 \tau^4}{120} \langle \mathbf{D}^5 \mathcal{H}^{n+\frac{1}{2}}, \mathcal{E}^{n+\frac{1}{2}} \rangle_h = \langle \Psi^{n+\frac{1}{2}}, \mathcal{E}^{n+\frac{1}{2}} \rangle_h. \end{aligned} \quad (5.21)$$

Adding (5.20) to (5.21) and making use of the complete square formulation, then, we can gain the following energy identity

$$\begin{aligned} \|\sqrt{\mu} \mathcal{H}^{n+1} - \frac{\tau}{2\sqrt{\mu}} \Phi^{n+\frac{1}{2}}\|_h^2 + \|\sqrt{\epsilon} \mathcal{E}^{n+1} - \frac{\tau}{2\sqrt{\epsilon}} \Psi^{n+\frac{1}{2}}\|_h^2 \\ = \|\sqrt{\mu} \mathcal{H}^n + \frac{\tau}{2\sqrt{\mu}} \Phi^{n+\frac{1}{2}}\|_N^2 + \|\sqrt{\epsilon} \mathcal{E}^n + \frac{\tau}{2\sqrt{\epsilon}} \Psi^{n+\frac{1}{2}}\|_h^2. \end{aligned} \quad (5.22)$$

With the use of the triangle inequality of the norm and (5.22), we can get

$$\begin{aligned} & \left( \|\sqrt{\mu} \mathcal{H}^{n+1}\|_h^2 + \|\sqrt{\epsilon} \mathcal{E}^{n+1}\|_h^2 \right)^{\frac{1}{2}} \\ & \leq \left( \|\sqrt{\mu} \mathcal{H}^{n+1} - \frac{\tau}{2\sqrt{\mu}} \Phi^{n+\frac{1}{2}}\|_h^2 + \|\sqrt{\epsilon} \mathcal{E}^{n+1} - \frac{\tau}{2\sqrt{\epsilon}} \Psi^{n+\frac{1}{2}}\|_h^2 \right)^{\frac{1}{2}} + \frac{\tau}{2} \left( \left\| \frac{1}{\sqrt{\mu}} \Phi^{n+\frac{1}{2}} \right\|_h^2 + \left\| \frac{1}{\sqrt{\epsilon}} \Psi^{n+\frac{1}{2}} \right\|_h^2 \right)^{\frac{1}{2}} \\ & = \left( \|\sqrt{\mu} \mathcal{H}^n + \frac{\tau}{2\sqrt{\mu}} \Phi^{n+\frac{1}{2}}\|_h^2 + \|\sqrt{\epsilon} \mathcal{E}^n + \frac{\tau}{2\sqrt{\epsilon}} \Psi^{n+\frac{1}{2}}\|_h^2 \right)^{\frac{1}{2}} + \frac{\tau}{2} \left( \left\| \frac{1}{\sqrt{\mu}} \Phi^{n+\frac{1}{2}} \right\|_h^2 + \left\| \frac{1}{\sqrt{\epsilon}} \Psi^{n+\frac{1}{2}} \right\|_h^2 \right)^{\frac{1}{2}} \\ & \leq \left( \|\sqrt{\mu} \mathcal{H}^n\|_h^2 + \|\sqrt{\epsilon} \mathcal{E}^n\|_h^2 \right)^{\frac{1}{2}} + \tau \left( \left\| \frac{1}{\sqrt{\mu}} \Phi^{n+\frac{1}{2}} \right\|_h^2 + \left\| \frac{1}{\sqrt{\epsilon}} \Psi^{n+\frac{1}{2}} \right\|_h^2 \right)^{\frac{1}{2}}. \end{aligned}$$

Recursively, applying the above inequality from time level  $n-1$  to 0, we have

$$\begin{aligned} \left( \|\sqrt{\mu} \mathcal{H}^n\|_h^2 + \|\sqrt{\epsilon} \mathcal{E}^n\|_h^2 \right)^{\frac{1}{2}} & \leq \left( \|\sqrt{\mu} \mathcal{H}^0\|_h^2 + \|\sqrt{\epsilon} \mathcal{E}^0\|_N^2 \right)^{\frac{1}{2}} \\ & + \sum_{l=0}^{n-1} \tau \left( \left\| \frac{1}{\sqrt{\mu}} \Phi^{l+\frac{1}{2}} \right\|_h^2 + \left\| \frac{1}{\sqrt{\epsilon}} \Psi^{l+\frac{1}{2}} \right\|_h^2 \right)^{\frac{1}{2}}. \end{aligned} \quad (5.23)$$

By virtue of Lemma 5.3, and recalling that  $\mathbf{H}^0 = \mathbf{H}(0)$ ,  $\mathbf{E}^0 = \mathbf{E}(0)$ , we have

$$\|\mathcal{H}^0\|_h = \|\mathbf{H}(0) - P_{N-2} \mathbf{H}(0)\|_h \leq CN^{-r},$$

and

$$\|\mathcal{E}^0\|_h = \|\mathbf{E}(0) - P_{N-2} \mathbf{E}(0)\|_h \leq CN^{-r},$$

which further implies that

$$\left( \|\sqrt{\mu} \mathcal{H}^0\|_h^2 + \|\sqrt{\epsilon} \mathcal{E}^0\|_h^2 \right)^{\frac{1}{2}} \leq CN^{-r}. \quad (5.24)$$

With noting  $n\tau < T$ , we can deduce from (5.23) and (5.24) that

$$\left( \|\sqrt{\mu} \mathcal{H}^n\|_h^2 + \|\sqrt{\epsilon} \mathcal{E}^n\|_h^2 \right)^{\frac{1}{2}} \leq CT(\tau^6 + N^{-r}), \quad n = 0, \dots, M. \quad (5.25)$$



Making use of (5.25) and the inequation,  $a + b \leq \sqrt{2a^2 + 2b^2}$ ,  $\forall a, b \geq 0$ , we can obtain

$$\|\sqrt{\mu}\mathcal{H}^n\|_h + \|\sqrt{\epsilon}\mathcal{E}^n\|_h \leq CT(\tau^6 + N^{-r}), \quad n = 0, \dots, M. \quad (5.26)$$

With Lemma 5.3 and Eq. (5.26), the following error estimate can be established

$$\begin{aligned} & \left( \mu \|\mathbf{H}(t_n) - \mathbf{H}^n\|_h^2 + \epsilon \|\mathbf{E}(t_n) - \mathbf{E}^n\|_h^2 \right)^{\frac{1}{2}} \leq \sqrt{\mu} \|\mathbf{H}(t_n) - \mathbf{H}^n\|_h + \sqrt{\epsilon} \|\mathbf{E}(t_n) - \mathbf{E}^n\|_h \\ & \leq \sqrt{\mu} \|\mathbf{H}(t_n) - P_{N-2}\mathbf{H}(t_n)\|_h + \sqrt{\mu} \|\mathcal{H}^n\|_h + \sqrt{\epsilon} \|\mathbf{E}(t_n) - P_{N-2}\mathbf{E}(t_n)\|_h + \sqrt{\epsilon} \|\mathcal{E}^n\|_h \\ & \leq CT(\tau^6 + N^{-r}), \quad n = 0, \dots, M. \end{aligned}$$

This ends the proof.  $\square$

## 6 Numerical dispersion relation

In this section, the numerical dispersion relation of the sixth order energy-conserved scheme (3.13) will be investigated. Let the elements of  $\mathbf{u}$  satisfy  $u_j = u_{j+N_w}$  with  $u_j = u_0 e^{-i\kappa_w j h_w}$ , and denote  $[(\mathbf{D}_1^w)^p]_{j,k} = (\hat{d}_p^w)_{j,k}$ ,  $[\mathbf{D}_p^w]_{j,k} = (d_p^w)_{j,k}$ , where  $j, k = 1, \dots, N_w$ . With the help of Lemmas 3.1-3.2 and Eq. (3.3), for a fixed positive integer  $p$ , we can obtain the following results:

When  $p$  is an odd integer, we have

$$\begin{aligned} [(\mathbf{D}_1^w)^p \mathbf{u}]_j &= \sum_{k=1}^{N_w} (\hat{d}_p^w)_{j,k} u_k = \sum_{k=1}^{N_w} (\hat{d}_p^w)_{j,j+k} u_{j+k} \\ &= \sum_{k=1}^{\frac{N_w}{2}-1} (\hat{d}_p^w)_{j,j+k} u_{j+k} + \sum_{k=\frac{N_w}{2}+1}^{N_w} (\hat{d}_p^w)_{j,j+k} u_{j+k} \\ &= \sum_{k=1}^{\frac{N_w}{2}-1} (\hat{d}_p^w)_{j,j+k} u_{j+k} + \sum_{k=-\frac{N_w}{2}+1}^0 (\hat{d}_p^w)_{j,j+k} u_{j+k} \\ &= \sum_{k=j-\frac{N_w}{2}+1}^{j+\frac{N_w}{2}-1} (\hat{d}_p^w)_{j,k} u_k = \sum_{k=j-\frac{N_w}{2}+1}^{j-1} (\hat{d}_p^w)_{j,k} u_k + \sum_{k=j+1}^{j+\frac{N_w}{2}-1} (\hat{d}_p^w)_{j,k} u_k \\ &= -2iu_0 e^{-i\kappa_w j h_w} \sum_{k=1}^{\frac{N_w}{2}-1} (\hat{d}_p^w)_{j,j+k} \sin(k h_w \kappa_w) \\ &= -2iu_0 e^{-i\kappa_w j h_w} \sum_{k=1}^{\frac{N_w}{2}-1} (d_p^w)_{j,j+k} \sin(k h_w \kappa_w) = u_0 e^{-i\kappa_w j h_w} \bar{d}_p^w, \end{aligned} \quad (6.1)$$

and

$$[\mathbf{D}_p^w \mathbf{u}]_j = -2iu_0 e^{-i\kappa_w j h_w} \sum_{k=1}^{\frac{N_w}{2}-1} (d_p^w)_{j,j+k} \sin(k h_w \kappa_w) = u_0 e^{-i\kappa_w j h_w} \tilde{d}_p^w, \quad (6.2)$$

where  $\bar{d}_p^w = \tilde{d}_p^w = -2i \sum_{k=1}^{\frac{N_w}{2}-1} (d_p^w)_{j,j+k} \sin(k h_w \kappa_w)$  is a pure imaginary number.

When  $p$  is an even integer, by the analogous argument, we have

$$[(\mathbf{D}_1^w)^p \mathbf{u}]_j = \sum_{k=1}^{N_w} (\hat{d}_p^w)_{j,k} u_k$$

$$\begin{aligned}
&= u_0 e^{-i\kappa_w j h_w} \left[ 2 \sum_{k=1}^{\frac{N_w}{2}-1} (\hat{d}_p^w)_{j,j+k} \cos(\kappa_w h_w k) \right. \\
&\quad \left. + (\hat{d}_p^w)_{j,j} + (\hat{d}_p^w)_{j,j+\frac{N_w}{2}} \cos(\kappa_w h_w N_w/2) \right] \\
&= u_0 e^{-i\kappa_w j h_w} \bar{d}_p^w,
\end{aligned} \tag{6.3}$$

and

$$\begin{aligned}
[\mathbf{D}_p^w \mathbf{u}]_j &= u_0 e^{-i\kappa_w j h_w} \left[ 2 \sum_{k=1}^{\frac{N_w}{2}-1} (d_p^w)_{j,j+k} \cos(\kappa_w h_w k) \right. \\
&\quad \left. + (d_p^w)_{j,j} + (d_p^w)_{j,j+\frac{N_w}{2}} \cos(\kappa_w h_w N_w/2) \right] \\
&= u_0 e^{-i\kappa_w j h_w} \tilde{d}_p^w,
\end{aligned} \tag{6.4}$$

where  $\bar{d}_p^w = 2 \sum_{k=1}^{\frac{N_w}{2}-1} (\hat{d}_p^w)_{j,j+k} \cos(\kappa_w h_w k) + (\hat{d}_p^w)_{j,j} + (\hat{d}_p^w)_{j,j+\frac{N_w}{2}} \cos(\kappa_w h_w N_w/2)$  and  $\tilde{d}_p^w = 2 \sum_{k=1}^{\frac{N_w}{2}-1} (d_p^w)_{j,j+k} \cos(\kappa_w h_w k) + (d_p^w)_{j,j} + (d_p^w)_{j,j+\frac{N_w}{2}} \cos(\kappa_w h_w N_w/2)$  are real numbers.

**Remark 6.1.** *The numerical dispersion relation of the proposed scheme (3.13) will be established, when  $\bar{d}_p^w$ ,  $p = 1, 2, 3, 4$  are obtained from Eqs. (6.1) and (6.3), respectively. Further, by virtue of Eqs. (6.1)-(6.3), the numerical dispersion relation of the Fourier pseudo-spectral method for generally linear Hamiltonian PDEs can also be well established.*

Take a plane wave solution of the Maxwell's equations (2.1) as

$$\begin{pmatrix} \mathbf{H} \\ \mathbf{E} \end{pmatrix} = \begin{pmatrix} \mathbf{H}_0 \\ \mathbf{E}_0 \end{pmatrix} e^{-i(k_x x + k_y y + k_z z - \omega t)}, \tag{6.5}$$

where  $\mathbf{H}_0 = ((H_x)_0, (H_y)_0, (H_z)_0)^T$ ,  $\mathbf{E}_0 = ((E_x)_0, (E_y)_0, (E_z)_0)^T$  denote an arbitrary constant vector,  $\omega$  is the frequency and  $k_x$ ,  $k_y$  and  $k_z$  are the wave number along the  $x$ -direction,  $y$ -direction and  $z$ -direction, respectively. Substituting (6.5) into the Maxwell's equations Eq. (2.1) leads to the exact dispersion relation

$$\omega^2 = c^2(k_x^2 + k_y^2 + k_z^2). \tag{6.6}$$

Associated with the dispersion relation is two important quantities: the phase velocity  $v_p$  and the group velocity  $v_g$

$$v_p = \frac{\omega}{|\boldsymbol{\kappa}|} \hat{\boldsymbol{\kappa}}, \quad v_g = \nabla_{\boldsymbol{\kappa}} \omega(\boldsymbol{\kappa}), \tag{6.7}$$

where the wave number vector  $\boldsymbol{\kappa} = (\kappa_x, \kappa_y, \kappa_z)$ , and  $\hat{\boldsymbol{\kappa}} = \frac{\boldsymbol{\kappa}}{|\boldsymbol{\kappa}|}$  is the unit vector. The phase velocity  $v_p$  describes the speed at which the phase of a wave propagate and the direction of the normal vector to the propagating wavefront. The group velocity  $v_g$  describes the speed at which the envelope of a wave packet propagates and gives the direction of the normal vector to the constant  $\omega$ -surface of the dispersion relation [46]. Here, we discuss the three dimensional problem in  $(x, y, z)$ . The exact group velocity  $v_g$  and the wave number vector  $\boldsymbol{\kappa}$  can be expressed as in spherical coordinates

$$v_g = |v_g|(\sin \alpha \cos \beta, \sin \alpha \sin \beta, \cos \alpha), \tag{6.8}$$

$$\boldsymbol{\kappa} = (\kappa_x, \kappa_y, \kappa_z) = |\boldsymbol{\kappa}|(\sin \phi \cos \theta, \sin \phi \sin \theta, \cos \phi), \tag{6.9}$$

where  $|v_g|$  and  $\alpha, \beta$  are the magnitude and angles of  $v_g$ , respectively,  $|\boldsymbol{\kappa}|$  and  $\theta, \phi$  are the magnitude and angles of  $\boldsymbol{\kappa}$ , respectively.

Next, we take the numerical solution of (2.1) to be

$$U_{w,j,k,m}^n = (U_w)_0 e^{-i(k_x j h_x + k_y k h_y + k_z m h_z - n \tau \omega)}, \quad U = H \text{ or } E, \quad (6.10)$$

where

$$-\pi \leq h_x \kappa_x \leq \pi, \quad -\pi \leq h_y \kappa_y \leq \pi, \quad -\pi \leq h_z \kappa_z \leq \pi, \quad -\pi \leq \tau \omega \leq \pi.$$

Let the increasing factor  $\lambda = e^{i\omega\tau}$ . Substituting

$$U_{w,j,k,m}^n = (U_w)_0 \lambda^n e^{-i(k_x j h_x + k_y k h_y + k_z m h_z)}, \quad U = H \text{ or } E, \quad (6.11)$$

into the component form of the scheme (3.14), then, we can obtain

$$\lambda \begin{pmatrix} \mathbf{I}_{3 \times 3} & c_1 \mathbf{A} \\ -c_2 \mathbf{A} & \mathbf{I}_{3 \times 3} \end{pmatrix} \begin{pmatrix} \mathbf{H}_0 \\ \mathbf{E}_0 \end{pmatrix} = \begin{pmatrix} \mathbf{I}_{3 \times 3} & -c_1 \mathbf{A} \\ c_2 \mathbf{A} & \mathbf{I}_{3 \times 3} \end{pmatrix} \begin{pmatrix} \mathbf{H}_0 \\ \mathbf{E}_0 \end{pmatrix}, \quad (6.12)$$

with  $c_1 = \frac{\tau}{2\mu}$ ,  $c_2 = \frac{\tau}{2\epsilon}$ , and

$$\mathbf{A} = \begin{pmatrix} 0 & -a_z & a_y \\ a_z & 0 & -a_x \\ -a_y & a_x & 0 \end{pmatrix},$$

where

$$\begin{aligned} a_x &= \bar{d}_1^x - \frac{c^2 \tau^2}{12} (\bar{d}_3^x + \bar{d}_1^x (\bar{d}_2^y + \bar{d}_2^z)) \\ &\quad + \frac{c^4 \tau^4}{120} (\bar{d}_5^x + \bar{d}_1^x (\bar{d}_4^y + 2\bar{d}_2^y \bar{d}_2^z + \bar{d}_4^z) + 2\bar{d}_3^x (\bar{d}_2^y + \bar{d}_2^z)), \end{aligned} \quad (6.13)$$

$a_w, w = y, z$  can be obtained by exchanging the index  $x \longleftrightarrow w$  in  $a_x$ , and

$$\begin{aligned} \bar{d}_1^w &= 2i \sum_{k=1}^{\frac{N_w}{2}-1} \left[ \frac{(-1)^k \pi}{N_w h_w} \cot\left(\frac{k\pi}{N_w}\right) \sin(k h_w \kappa_w) \right], \\ \bar{d}_2^w &= \left[ N_w - \frac{N_w^2 + 2}{3} + (-1)^{\frac{N_w}{2}} (N_w - 2) \cos\left(\frac{N_w}{2} h_w \kappa_w\right) \right] \left( \frac{\pi}{N_w h_w} \right)^2 \\ &\quad + \sum_{k=1}^{\frac{N_w}{2}-1} (-1)^k \left[ \frac{2\pi^2}{N_w h_w^2} - \left( \frac{2\pi}{N_w h_w} \right)^2 \csc^2\left(\frac{k\pi}{N_w}\right) \right] \cos(k h_w \kappa_w), \\ \bar{d}_3^w &= -2i \sum_{k=1}^{\frac{N_w}{2}-1} \frac{(-1)^k}{N_w} \left( \frac{\pi}{h_w} \right)^3 \left[ \cot\left(\frac{k\pi}{N_w}\right) - \frac{6}{N_w^2} \cos\left(\frac{k\pi}{N_w}\right) \csc^3\left(\frac{k\pi}{N_w}\right) \right] \sin(k h_w \kappa_w), \\ \bar{d}_4^w &= \left( \frac{\pi}{h_w} \right)^4 \left[ \frac{1}{5} - \frac{1}{N_w} + \frac{4}{3N_w^2} - \frac{8}{15N_w^4} + (-1)^{\frac{N_w}{2}} \left( \frac{4}{N_w^2} - \frac{8}{N_w^4} - \frac{1}{N_w} \right) \cos\left(\frac{N_w}{2} h_w \kappa_w\right) \right] \\ &\quad + 2 \sum_{k=1}^{\frac{N_w}{2}-1} (-1)^k \left( \frac{\pi}{h_w} \right)^4 \left[ \csc^2\left(\frac{k\pi}{N_w}\right) \left( \frac{4}{N_w^2} - \frac{8}{N_w^4} - \frac{24}{N_w^4} \cot^2\left(\frac{k\pi}{N_w}\right) \right) - \frac{1}{N_w} \right] \cos(k h_w \kappa_w), \\ \bar{d}_5^w &= 2i \sum_{k=1}^{\frac{N_w}{2}-1} (-1)^k \left( \frac{\pi}{h_w} \right)^5 \cot\left(\frac{k\pi}{N_w}\right) \left[ \frac{1}{N_w} + \frac{20}{N_w^5} \csc^2\left(\frac{k\pi}{N_w}\right) \left( 4 + 6 \cot^2\left(\frac{k\pi}{N_w}\right) - N_w^2 \right) \right] \\ &\quad \sin(k h_w \kappa_w). \end{aligned}$$

Since Eq. (6.12) holds for nonzero  $U_{w_0}$ , this implies that

$$|\lambda \mathbf{I}_{6 \times 6} - \mathcal{A}^{-1}(2\mathbf{I}_{6 \times 6} - \mathcal{A})| = 0, \quad (6.14)$$

where

$$\mathcal{A} = \begin{pmatrix} \mathbf{I}_{3 \times 3} & c_1 \mathbf{A} \\ -c_2 \mathbf{A} & \mathbf{I}_{3 \times 3} \end{pmatrix}.$$

By careful calculation, we have

$$\begin{aligned} \lambda_{1,2} &= 1, \quad \lambda_{3,4} = \frac{1 + i\sqrt{c_1 c_2} \sqrt{|a_x|^2 + |a_y|^2 + |a_z|^2}}{1 - i\sqrt{c_1 c_2} \sqrt{|a_x|^2 + |a_y|^2 + |a_z|^2}}, \\ \lambda_{5,6} &= \frac{1 - i\sqrt{c_1 c_2} \sqrt{|a_x|^2 + |a_y|^2 + |a_z|^2}}{1 + i\sqrt{c_1 c_2} \sqrt{|a_x|^2 + |a_y|^2 + |a_z|^2}}. \end{aligned} \quad (6.15)$$

It follows from (6.15) that the modulus of the characteristic values are equal to one. Therefore, we have the following theorem.

**Theorem 6.1.** *The proposed sixth order energy-conserved scheme is unconditionally stable and non-dissipative.*

Sequentially, inserting  $\lambda = e^{i\omega\tau}$  into the characteristic values (6.15) results in numerical dispersion relation of the scheme (3.13)

$$\tan^2 \frac{\omega\tau}{2} = \frac{\tau^2 c^2}{4} (|a_x|^2 + |a_y|^2 + |a_z|^2). \quad (6.16)$$

It is remarked that the dispersion relation (6.16) converges to the theoretical dispersion relation (6.6) provided that  $\tau, h_x, h_y, h_z \rightarrow 0$ .

Then, the normalized phase velocity is given by

$$\left| \frac{v_p}{c} \right| = \left| \frac{\omega}{c|\kappa|} \right|, \quad (6.17)$$

It is obvious that the normalized phase velocity of the Maxwell's equations (2.1) is equal to one. Supposing  $N_x = N_y = N_z = N$ ,  $S = c\frac{\tau}{h}$  and the number of points per wavelength  $N_\lambda = \frac{\lambda}{h}$  ( $\lambda$  is the wavelength), the normalized phase velocity of the scheme (3.13) can be expressed as

$$\left| \frac{v_p}{c} \right| = \frac{N_\lambda}{\pi S} \tan^{-1} \left( \frac{1}{2} \sqrt{|c\tau a_x|^2 + |c\tau a_y|^2 + |c\tau a_z|^2} \right). \quad (6.18)$$

Finally, we calculate the magnitude of the group velocity  $v_g$  by

$$|v_g| = \sqrt{(v_g)_x^2 + (v_g)_y^2 + (v_g)_z^2} = \sqrt{\left( \frac{\partial \omega}{\partial \kappa_x} \right)^2 + \left( \frac{\partial \omega}{\partial \kappa_y} \right)^2 + \left( \frac{\partial \omega}{\partial \kappa_z} \right)^2}. \quad (6.19)$$

It's clear that the exact group velocity of the Maxwell's equations (2.1) is equal to one. From numerical dispersion relation (6.16), we have

$$\frac{\partial \omega}{\partial \kappa_w} = \mathbb{A} \frac{\partial (|a_x|^2 + |a_y|^2 + |a_z|^2)}{\partial \kappa_w} = -\mathbb{A} \left( \frac{\partial a_x^2}{\partial \kappa_w} + \frac{\partial a_y^2}{\partial \kappa_w} + \frac{\partial a_z^2}{\partial \kappa_w} \right), \quad (6.20)$$

where

$$\mathbb{A} = \frac{c}{2} \frac{1}{[1 + (\frac{c\tau}{2})^2 (|a_x|^2 + |a_y|^2 + |a_z|^2)] \sqrt{|a_x|^2 + |a_y|^2 + |a_z|^2}}, \quad (6.21)$$

and

$$\begin{aligned} \frac{\partial a_x^2}{\partial \kappa_x} = & 2a_x \left\{ \frac{\partial \bar{d}_1^x}{\partial \kappa_x} - \frac{c^2 \tau^2}{12} \left[ \frac{\partial \bar{d}_3^x}{\partial \kappa_x} + \frac{\partial \bar{d}_1^x}{\partial \kappa_x} (\bar{d}_2^y + \bar{d}_2^z) \right] \right. \\ & \left. + \frac{c^4 \tau^4}{120} \left[ \frac{\partial \bar{d}_5^x}{\partial \kappa_x} + \frac{\partial \bar{d}_1^x}{\partial \kappa_x} (\bar{d}_4^y + 2\bar{d}_2^y \bar{d}_2^z + \bar{d}_4^z) + 2 \frac{\partial \bar{d}_3^x}{\partial \kappa_x} (\bar{d}_2^y + \bar{d}_2^z) \right] \right\}, \end{aligned} \quad (6.22)$$

$$\frac{\partial a_x^2}{\partial \kappa_y} = 2a_x \left\{ -\frac{c^2 \tau^2}{12} \bar{d}_1^x \frac{\partial \bar{d}_2^y}{\partial \kappa_y} + \frac{c^4 \tau^4}{120} \left[ (2\bar{d}_1^x \bar{d}_2^z + 2\bar{d}_3^x) \frac{\partial \bar{d}_2^y}{\partial \kappa_y} + \bar{d}_1^x \frac{\partial \bar{d}_4^y}{\partial \kappa_y} \right] \right\}. \quad (6.23)$$

Others can be obtained by the following tricks

1.  $\frac{\partial a_w^2}{\partial \kappa_w}$ ,  $w = y, z$  are obtained by exchanging  $x \longleftrightarrow w$  in Eq. (6.22),
2.  $\frac{\partial a_y^2}{\partial \kappa_x}$ ,  $\frac{\partial a_z^2}{\partial \kappa_x}$  and  $\frac{\partial a_z^2}{\partial \kappa_y}$  are obtained by exchanging  $y \longleftrightarrow x$ ,  $y \longleftrightarrow z$  and  $x \longleftrightarrow z$  in Eq. (6.23), respectively.
3.  $\frac{\partial a_z^2}{\partial \kappa_x}$  and  $\frac{\partial a_y^2}{\partial \kappa_z}$  are obtained by exchanging  $y \longleftrightarrow z$  in  $\frac{\partial a_y^2}{\partial \kappa_x}$  and  $x \longleftrightarrow y$  in  $\frac{\partial a_x^2}{\partial \kappa_z}$ , respectively.

Thus, the numerical group velocity of the scheme (3.13) can be obtained by inserting  $\frac{\partial \omega}{\partial \kappa_w}$ ,  $w = x, y, z$  into Eq. (6.19).

## 7 Numerical experiments

In this section, we will investigate the numerical behavior of the proposed method (3.13) presented in Section 3 and analyze the numerical dispersion relation derived in Section 4. All diagrams presented below refer to the numerical integration of the Maxwell's equations (2.1) with  $\mu = \epsilon = 1$ .

### 7.1 Benchmark test

In this subsection, we will focus on the rate of convergence, the two divergence-free properties as well as the discrete energy and momentum conservation laws. Furthermore, some comparisons between our scheme and the composition scheme which is derived from the composition method (see Page. 44 in Ref. [20]) via the AVF scheme in Ref. [6] and the Gauss scheme obtained by using the Gauss methods of order 6 (see Page. 34 in Ref. [20]) for Eq. (3.6) will be presented. In our computations, a fast solver is employed to solve the linear system (3.13) efficiently. For more details of the fast solver, please refer to Appendix. We assume that the domain is  $\Omega = [0, 2] \times [0, 2] \times [0, 2]$  with periodic boundary conditions. The exact solutions of Eqs. (2.1) are [13]

$$E_x = \frac{k_y - k_z}{\epsilon \sqrt{\mu w}} \cos(w\pi t) \cos(k_x \pi x) \sin(k_y \pi y) \sin(k_z \pi z), \quad (7.1)$$

$$H_x = \sin(w\pi t) \sin(k_x \pi x) \cos(k_y \pi y) \cos(k_z \pi z), \quad (7.2)$$

$$E_y = \frac{k_z - k_x}{\epsilon \sqrt{\mu w}} \cos(w\pi t) \sin(k_x \pi x) \cos(k_y \pi y) \sin(k_z \pi z), \quad (7.3)$$

$$H_y = \sin(w\pi t) \cos(k_x \pi x) \sin(k_y \pi y) \cos(k_z \pi z), \quad (7.4)$$

$$E_z = \frac{k_x - k_y}{\epsilon \sqrt{\mu w}} \cos(w\pi t) \sin(k_x \pi x) \sin(k_y \pi y) \cos(k_z \pi z), \quad (7.5)$$

$$H_z = \sin(w\pi t) \cos(k_x \pi x) \cos(k_y \pi y) \sin(k_z \pi z), \quad (7.6)$$

where  $k_x = 1, k_y = 2, k_z = -3$  and  $w = (k_x^2 + k_y^2 + k_z^2)/(\epsilon\mu)$ .

We set the exact solutions (6.1-6.6) at  $t = 0$  on the domain  $\Omega = [0, 2] \times [0, 2] \times [0, 2]$  as initial conditions. In order to evaluate the numerical errors, the following formulas are used

$$L^\infty = \max \left\{ \|\mu \mathbf{H}(t_n) - \mu \mathbf{H}^n\|_{h,\infty}, \|\epsilon \mathbf{E}(t_n) - \epsilon \mathbf{E}^n\|_{h,\infty} \right\}, \quad (7.7)$$

and

$$L^2 = (\mu \|\mathbf{H}(t_n) - \mathbf{H}^n\|_h^2 + \epsilon \|\mathbf{E}(t_n) - \mathbf{E}^n\|_h^2)^{\frac{1}{2}}. \quad (7.8)$$

The rate of convergence is defined as

$$\text{Rate} = \frac{\ln(\text{error}_1/\text{error}_2)}{\ln(\tau_1/\tau_2)}, \quad (7.9)$$

where  $\tau_l, \text{error}_l, (l = 1, 2)$  are step sizes and errors with the step size  $\tau_l$ , respectively.

**Table. 1:** The temporal errors and rates of convergence of different schemes with different time steps and  $N_x = N_y = N_z = 16$  at  $T = 1$ .

Scheme	$\tau$	$L^\infty$	Rate	$L^2$	Rate	CPU (s)
(3.13)	0.01	2.5295e-08	-	4.5198e-08	-	0.6
	0.005	3.9585e-10	5.9978	7.0731e-10	5.9978	1.0
	0.0025	6.2084e-12	5.9946	1.1053e-11	5.9998	1.7
	0.00125	1.9063e-13	-	2.7046e-13	-	2.9
composition	0.01	7.3383e-08	-	1.3112e-07	-	1.3
	0.005	1.1481e-09	5.9981	2.0515e-09	5.9981	2.0
	0.0025	1.8013e-11	5.9941	3.2060e-11	5.9999	3.3
	0.00125	5.3180e-13	-	6.2894e-13	-	6.1
Gauss	0.01	2.9804e-10	-	5.3255e-10	-	2.0
	0.005	4.6428e-12	6.004	8.3228e-12	5.9997	2.7
	0.0025	9.3703e-14	5.6308	1.4772e-13	5.8161	3.9
	0.00125	8.3932e-14	-	1.4881e-13	-	6.2

**Table. 2:** The spatial error of the proposed scheme with different spatial steps and  $\tau = 10^{-3}$  at  $T = 1$ .

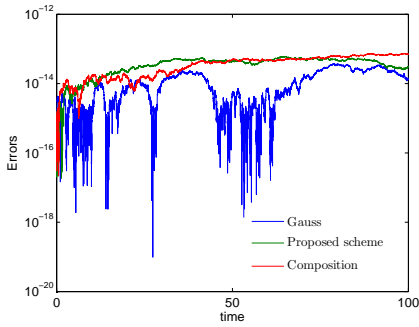
$N_x \times N_y \times N_z$	$L^\infty$	$L^2$	CPU (s)
$8 \times 8 \times 8$	8.8374e-13	1.0989e-13	1.5
$16 \times 16 \times 16$	1.1513e-13	1.3643e-13	3.8
$32 \times 32 \times 32$	1.7786e-13	2.2746e-13	33.1
$64 \times 64 \times 64$	1.9196e-13	2.4856e-13	450.1

Table 1 shows the temporal errors and rates of convergence of different schemes with different time steps and  $N_x = N_y = N_z = 16$  at  $T = 1$ . It is clear that all schemes can reach the theoretical order of 6, which verifies the theoretical analysis. Compared with the composition scheme, the proposed scheme shows distinct advantage in the errors and CPU time. The Gauss scheme provides smaller error than our scheme, but our scheme is the most efficient. In addition, since the Gauss scheme contains triple

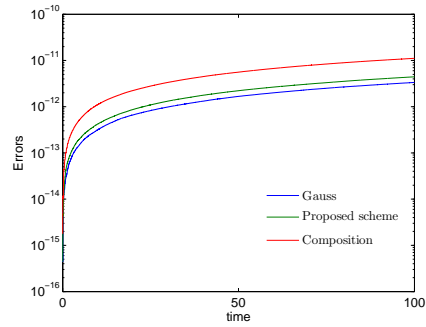
intermediate variables, the memory requirements of the Gauss scheme are at least triple as large as our scheme. We display the spatial error of the scheme (3.13) in Table 2. As illustrated in Table 2, the spatial error of the proposed scheme is negligible and up to machine precision, which confirms that, for sufficiently smooth problems, the Fourier pseudo-spectral method is of arbitrary order of accuracy. We omit the spatial error of the composition and Gauss schemes because they are also discretized by the Fourier pseudo-spectral method in space.

Then, we investigate the errors of the energy and momentum conservation laws over the time interval  $t \in [0, 100]$  with  $N_x = N_y = N_z = 16$  and  $\tau = 0.01$  in Fig. 1. It is clear to see that the errors on the energy and momentum of the Gauss scheme is the smallest, whereas, the ones of the composition scheme is the largest. It's worth noting that energy invariants  $\mathcal{E}_3$  and  $\mathcal{E}_{5x}$  are larger than others, we suspect that it is probably due to the fact that they have been divided by the time size  $\tau$  at each time level. The errors of the invariants  $\mathcal{E}_{4w}$ ,  $\mathcal{E}_{5w}$  and  $\mathcal{M}_w$ ,  $w = y, z$  are not presented since they are close to the case of  $x$ .

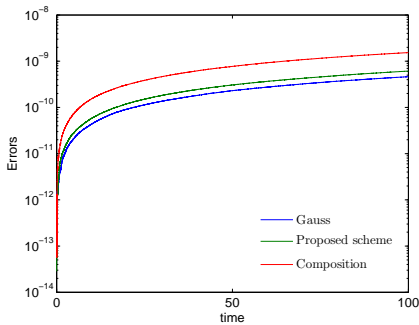
Finally, we check the two discrete divergence-free fields over the time interval  $t \in [0, 100]$  with  $N_x = N_y = N_z = 16$  and  $\tau = 0.01$  in Fig. 2. Numerical results show that the two discrete divergence-free fields reach machine precision in long time computation, which confirms the fact that, with appropriate collocation points, our scheme can preserve the two divergence-free fields exactly.



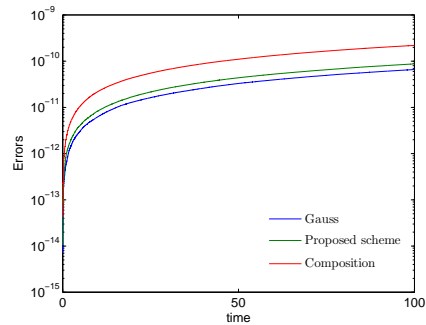
(a) Errors in invariant  $\mathcal{E}_1$ .



(b) Errors in invariant  $\mathcal{E}_2$ .



(c) Errors in invariant  $\mathcal{E}_3$ .



(d) Errors in invariant  $\mathcal{E}_{4x}$ .

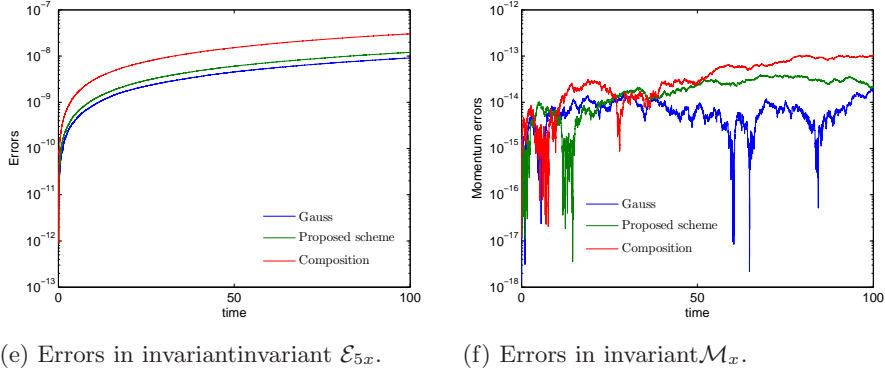


**Fig. 1:** The errors in invariants over the time interval  $t \in [0, 100]$  with  $N_x = N_y = N_z = 16$  and  $\tau = 0.01$ .

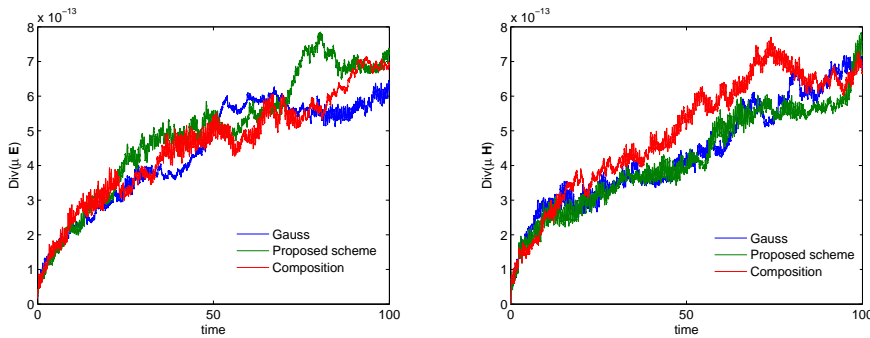


**Fig. 2:** The two discrete divergence-free fields over the time interval  $t \in [0, 100]$  with  $N_x = N_y = N_z = 16$  and  $\tau = 0.01$ .

## 7.2 Numerical dispersion analysis

In this subsection, we will investigate the numerical dispersion relation of the proposed method (3.13) including the numerical phase velocity and the numerical group velocity. In the following discussion, for the sake of simplicity, only uniform cell is considered, i.e.,  $N_x = N_y = N_z = N = 150$ .

### 7.2.1 Normalized numerical phase velocity

First, we will focus on the normalized numerical phase velocity by comparing our scheme (3.13) with the AVF(4) scheme [6]. Figs. 3 and 4 show the comparisons of normalized numerical phase velocities versus the Courant-Friedrich-Levy (CFL) number  $S$ , the number of points per wavelength  $N_\lambda$  and the propagation angles  $\phi$  and  $\theta$ . As illustrated in Figs. 3 and 4, the proposed scheme (3.13) is the best one whose normalized numerical phase velocity is the closest to the analytic solution one, which implies that the proposed method has lower numerical phase error than the AVF(4) scheme.



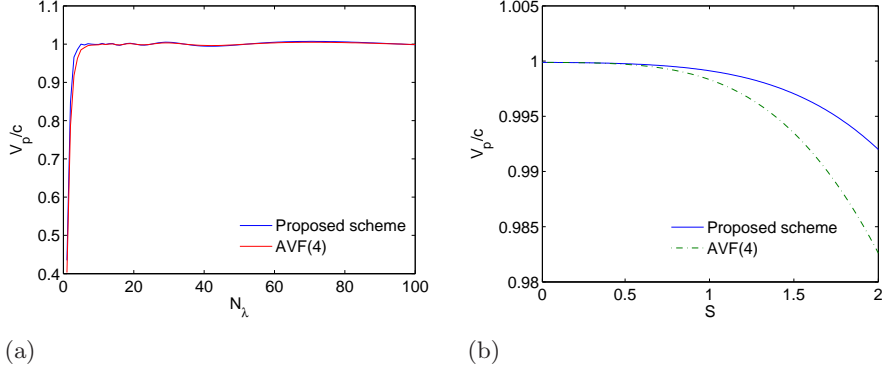


**Fig. 3:** (a) Normalized numerical phase velocities versus the number of points per wavelength  $N_\lambda$  with  $\phi = \pi/4$  and  $\theta = 3\pi/8$ . (b) Normalized numerical phase velocities versus the CFL number  $S$  with  $N_\lambda = 5$  with  $\phi = \pi/4$  and  $\theta = 3\pi/8$ .

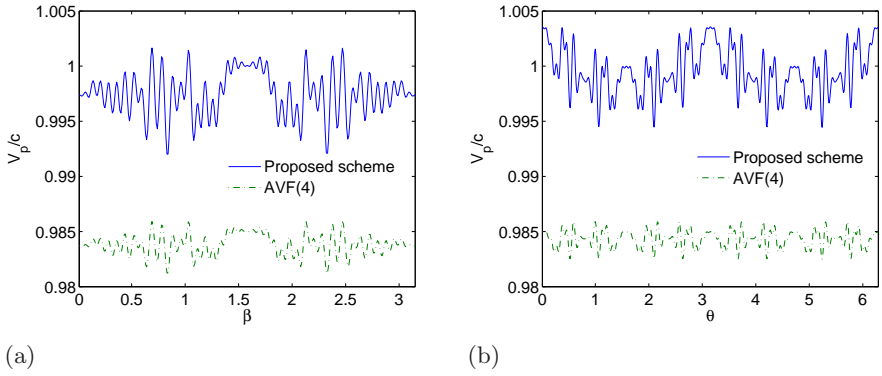
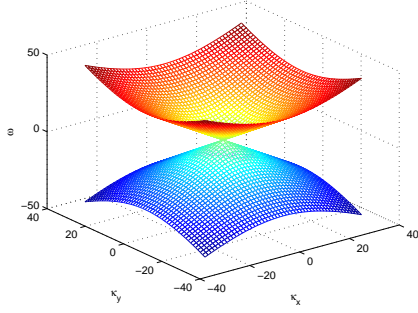


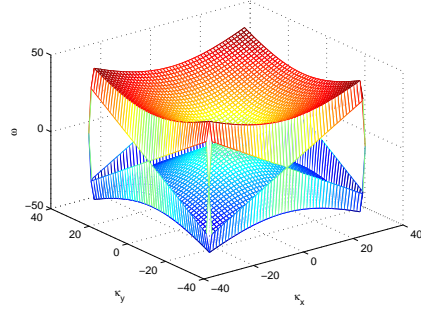
**Fig. 4:** (a) Normalized numerical phase velocities versus the propagation angles  $\phi$  with  $S = 1$ ,  $N_\lambda = 5$  and  $\theta = 3\pi/8$ . (b) Normalized numerical phase velocities versus the propagation angles with  $\theta$  with  $S = 1$ ,  $N_\lambda = 5$  and  $\phi = \pi/4$ .

### 7.2.2 Some analysis on the numerical dispersion relation

In this subsection, we make some analysis on the numerical dispersion relation of the proposed scheme (3.13). In Fig. 5, we first plot the dispersion relation for the frequency  $\omega$  as a function of the wave number vector  $(\kappa_x, \kappa_y)$ . From Fig. 5 (b), one can see that, similar to the conventional FDTD methods [7, 43], the proposed method (3.13) gives a numerical dispersion surface  $\omega$  with extra solution branches which correspond to the existence of the nonphysical parasitic waves in the numerical solution [2]. But, in contrast to the FDTD methods, such extra solution branches only occur with large wave numbers. This fact can be verified in following analysis again. In order to see the relation clearly, the contour plots of  $\omega$  are displayed in Fig 6. As illustrated in Fig 6 (b), we can observe that, except for the large wave numbers  $\kappa_w, w = x, y$ , the numerical contours are circular and the distances and shapes of the numerical contours are almost consistent with the exact one. This conforms the fact in Fig. 5 (b) and implies that the numerical propagation speed  $|v_g|$  is direction-independent. In addition, we can infer that the grid-anisotropy [45] of the scheme (3.13) causes that propagation directions  $\alpha$  and  $\beta$  (see (6.8)) are independent of the directions. Here, due to the symmetric property of the numerical dispersion relation, we omit the figures of the dispersion relation on the other planes.

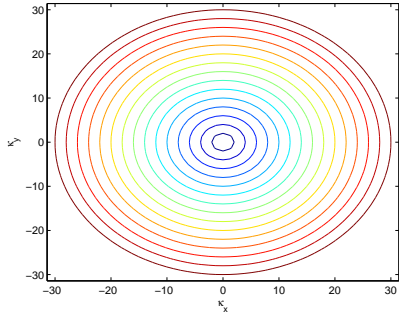


(a) Exact dispersion (6.6)

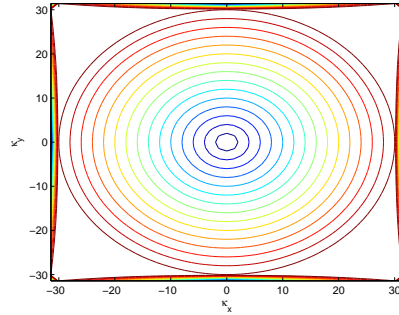


(b) Scheme (3.13)

**Fig. 5:** The dispersion relation figures on  $(\kappa_x, \kappa_y)$  with  $\tau = 0.01$ ,  $h = 0.1$  and  $N = 150$  for the Maxwell's equations.



(a) Exact dispersion (6.6)

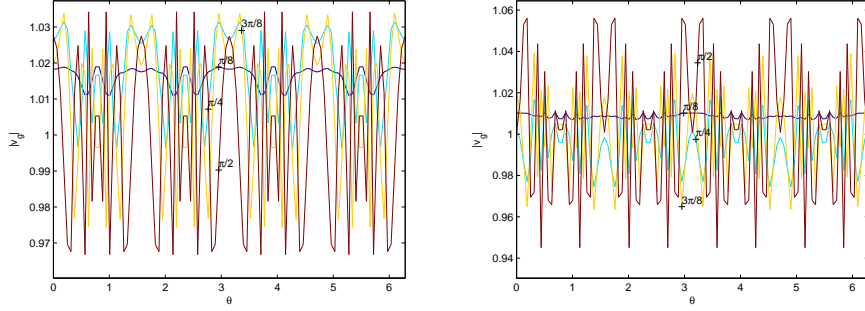


(b) Scheme (3.13)

**Fig. 6:** The contour plots on  $(\kappa_x, \kappa_y)$ -plane with  $\tau = 0.01$ ,  $h = 0.1$  and  $N = 150$  for the Maxwell's equations.

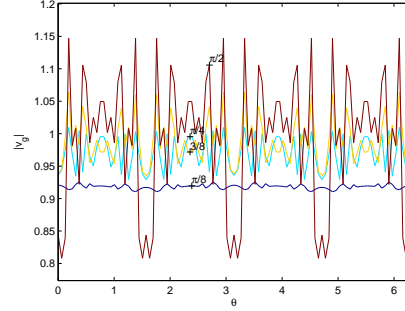
In order to verify the above inference, we investigate the magnitude  $|v_g|$  of the group velocity (6.19) in spherical coordinates (6.9). The group velocity, which characterizes the speed of energy transport in wave packets [46], is fundamental to the understanding of linear waves [46].

Fig. 7 shows the relation between the numerical group velocities and the wave number angles  $\theta$  at different  $|\kappa|$  and  $\phi$ . The group velocity, which characterizes the speed of energy transport in wave packets [46], is fundamental to the understanding of linear waves [46]. The relation between the numerical group velocities and the wave number angles  $\phi$  at different  $|\kappa|$  and  $\theta$  is displayed in Fig. 8.



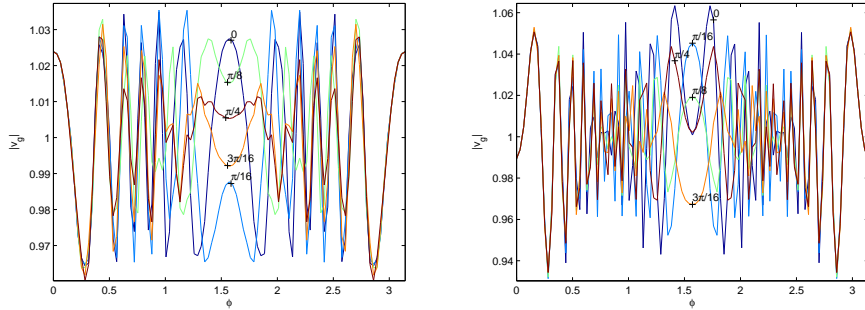
(a)  $|\kappa| = 2.5\pi$

(b)  $|\kappa| = 5\pi$



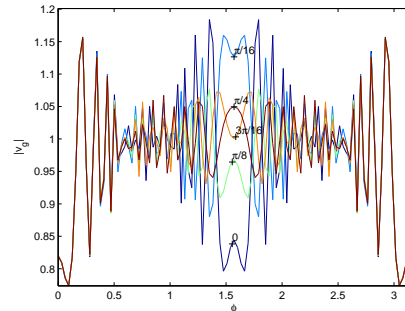
(c)  $|\kappa| = 7.5\pi$

**Fig. 7:** Numerical group velocities at different  $|\kappa|$  and  $\phi$  with  $\tau = 0.01$ ,  $h = 0.1$  and  $N = 150$  for the Maxwell's equations.



(a)  $|\kappa| = 2.5\pi$

(b)  $|\kappa| = 5\pi$



(c)  $|\kappa| = 7.5\pi$

**Fig. 8:** Numerical group velocities at different  $|\kappa|$  and  $\theta$  with  $\tau = 0.01$ ,  $h = 0.1$  and  $N = 150$  for the Maxwell's equations.

We can make some observations from the figures:

- (1) For all  $|\boldsymbol{\kappa}|$ , numerical group velocity occurs oscillation phenomena with exact value one. But it's worth noting that, in Fig. 7, for fixed  $\phi = \frac{\pi}{8}$ , when  $|\boldsymbol{\kappa}| = 2.5\pi$  or  $5\pi$ ,  $|v_g|$  is greater than the exact value one. However, for  $|\boldsymbol{\kappa}| = 7.5\pi$ ,  $|v_g|$  is less than one.
- (2) The maximum value of the numerical group velocity increases as  $|\boldsymbol{\kappa}|$  increases, which implies the magnitude of  $v_g$  depends on the vector wave number  $|\boldsymbol{\kappa}|$ . Therefore, the proposed scheme (3.13) is dispersive. That is, a wave-packet of this scheme with different  $|\boldsymbol{\kappa}|$  will spread out.
- (3) In Fig. 7, it is clear to see that the  $|v_g|$  is symmetric with respect to  $\theta = \pi$ . If dividing the domain of  $\theta$  into four equal parts  $[0, \frac{\pi}{2}]$ ,  $[\frac{\pi}{2}, \pi]$ ,  $[\pi, \frac{3\pi}{2}]$ , and  $[\frac{3\pi}{2}, 2\pi]$ , respectively, we can find that, whatever  $|\boldsymbol{\kappa}|$  and  $\phi$  chosen,  $v_g$  is symmetric with respect to  $\theta = \frac{\pi}{4}, \frac{3\pi}{4}, \frac{5\pi}{4}, \frac{7\pi}{4}$  in each part of the domain. Furthermore, from Fig. 8, we can observe that, whatever  $|\boldsymbol{\kappa}|$  chooses, the  $|v_g|$  is also symmetric with respect to  $\phi = \frac{\pi}{2}$  which means the  $(x, y)$ -plane.

We then calculate the propagation angles of the group velocity  $\alpha$  and  $\beta$ . Note that the exact dispersion relation is as follows

$$\begin{aligned} v_g &= |v_g| (\sin \alpha \cos \beta, \sin \alpha \sin \beta, \cos \alpha) = \left( \frac{\partial \omega}{\partial \kappa_x}, \frac{\partial \omega}{\partial \kappa_y}, \frac{\partial \omega}{\partial \kappa_z} \right) \\ &= \left( \frac{\kappa_x}{\omega}, \frac{\kappa_y}{\omega}, \frac{\kappa_z}{\omega} \right) = |\boldsymbol{\kappa}| \left( \frac{\sin \phi \cos \theta}{\omega}, \frac{\sin \phi \sin \theta}{\omega}, \frac{\cos \phi}{\omega} \right), \end{aligned} \quad (7.10)$$

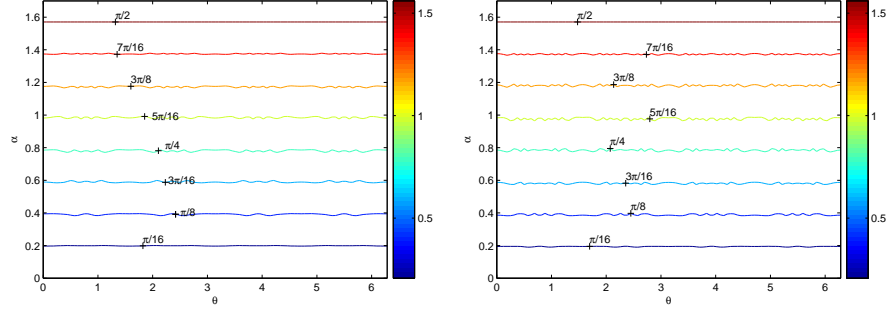
we can obtain  $\alpha = \phi$  and  $\beta = \theta$ . Similarly, by virtue of the numerical dispersion relation, we can derive

$$\alpha = \arctan \left( \sqrt{\frac{(\frac{\partial \omega}{\partial \kappa_x})^2 + (\frac{\partial \omega}{\partial \kappa_y})^2}{(\frac{\partial \omega}{\partial \kappa_z})^2}} \right), \quad (7.11)$$

$$\beta = \arctan \left( \frac{\frac{\partial \omega}{\partial \kappa_y}}{\frac{\partial \omega}{\partial \kappa_x}} \right), \quad (7.12)$$

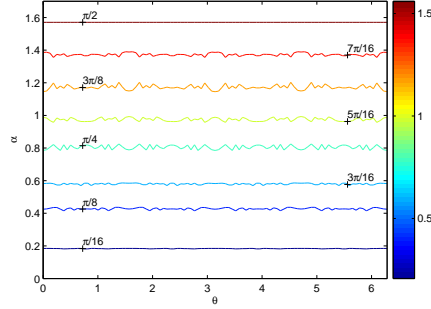
where  $\frac{\partial \omega}{\partial \kappa_x}$ ,  $\frac{\partial \omega}{\partial \kappa_y}$  and  $\frac{\partial \omega}{\partial \kappa_z}$  are defined as above.

Due to the symmetry of the  $\phi$  and the range value of the function arctan, we only need to consider  $\phi \in [0, \frac{\pi}{2}]$ , here. The relations between the propagation angle  $\alpha$  and the wave number angle  $\theta \in [0, 2\pi]$  with  $|\boldsymbol{\kappa}| = 2.5\pi$ ,  $|\boldsymbol{\kappa}| = 5\pi$  and  $|\boldsymbol{\kappa}| = 7.5\pi$  at different  $\phi \in [0, \frac{\pi}{2}]$  are plotted in Fig. 9. We can find the similar results about symmetry with respect to  $\theta$ . Thus, we just need to discuss the relation between  $\alpha$  and  $\phi$  in the domain  $[0, \frac{\pi}{2}]$  of  $\theta$ , which is represented by the contour plots in Fig. 10. Then, the relations between the propagation angle  $\beta$  and the wave number angle  $\phi \in [0, 2\pi]$  with  $|\boldsymbol{\kappa}| = 2.5\pi$ ,  $|\boldsymbol{\kappa}| = 5\pi$  and  $|\boldsymbol{\kappa}| = 7.5\pi$  at different  $\theta \in [0, \frac{\pi}{2}]$  are plotted in Fig. 11, which shows that whatever the  $\phi$  chosen, the  $\beta$  is symmetric with respect to  $\phi = \frac{\pi}{2}$ . This fact implies that we only need to discuss the relation between  $\beta$  and  $\theta$  in the domain  $[0, \frac{\pi}{2}]$  of  $\phi$ , which is displayed via contour plots in Fig. 12. As illustrated in Fig. 9, we can observe that, for a fixed angle  $\alpha$ , as the wave number  $|\boldsymbol{\kappa}|$  increases,  $\alpha$  does vary. In contrast, as the angle  $\theta$  vary,  $\alpha$  has almost no change. This implies that the angle  $\alpha$  only depends on the wave number  $|\boldsymbol{\kappa}|$  and is independent of the angle  $\theta$ . Similarly, as illustrated in Fig. 11, we can see that the angle  $\beta$  is independent of the angle  $\phi$  as well. We can confirm the facts again in Fig. 10 and Fig. 12 respectively. Now, we can conclude that the grid-anisotropy of the proposed method is direction-independent.



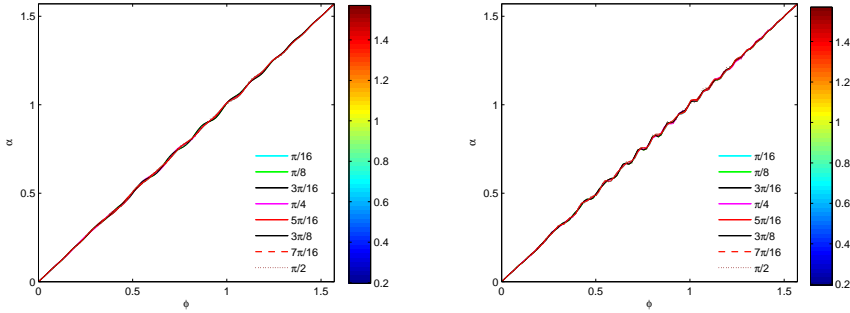
(a)  $|\kappa| = 2.5\pi$

(b)  $|\kappa| = 5\pi$



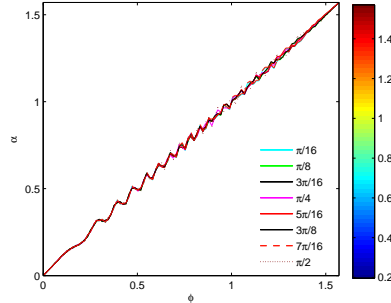
(c)  $|\kappa| = 7.5\pi$

**Fig. 9:** Wave propagation angle  $\alpha$  versus the wave number angle  $\theta$  and  $\phi$  at different  $|\kappa|$  with  $\tau = 0.01$ ,  $h = 0.1$  and  $N = 150$  for the Maxwell's equations.



(a)  $|\kappa| = 2.5\pi$

(b)  $|\kappa| = 5\pi$



(c)  $|\kappa| = 7.5\pi$

**Fig. 10:** Wave propagation angle  $\alpha$  versus the wave number angle  $\phi$  at different  $|\kappa|$  with  $\tau = 0.01$ ,  $h = 0.1$  and  $N = 150$  for the Maxwell's equations.

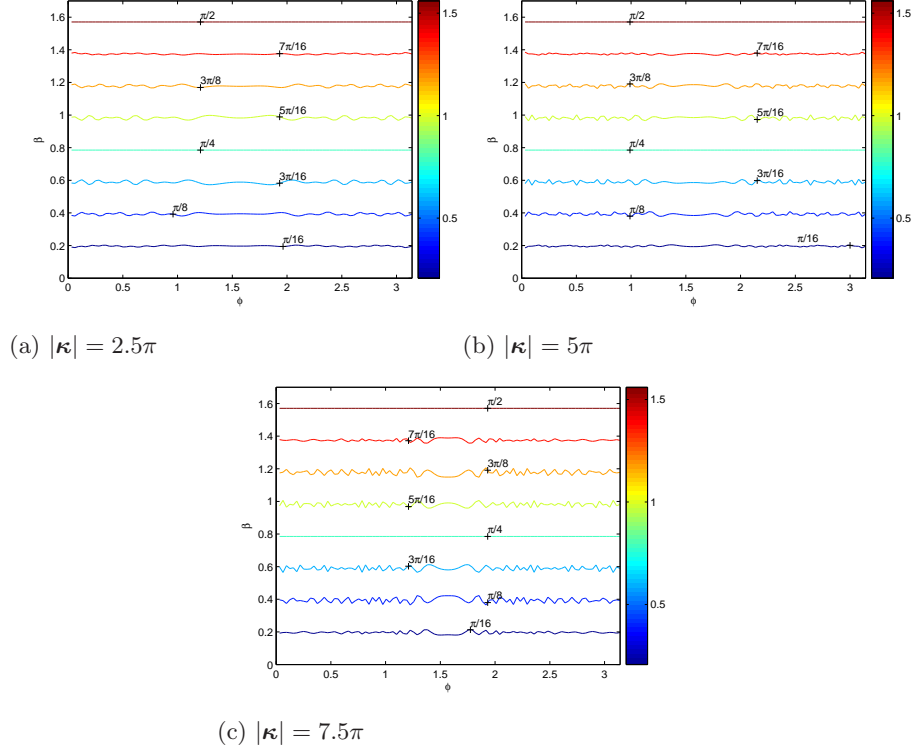


**Fig. 11:** Wave propagation angle  $\beta$  versus the wave number angle  $\phi$  and  $\theta$  at different  $|\kappa|$  with  $\tau = 0.01$ ,  $h = 0.1$  and  $N = 150$  for the Maxwell's equations.

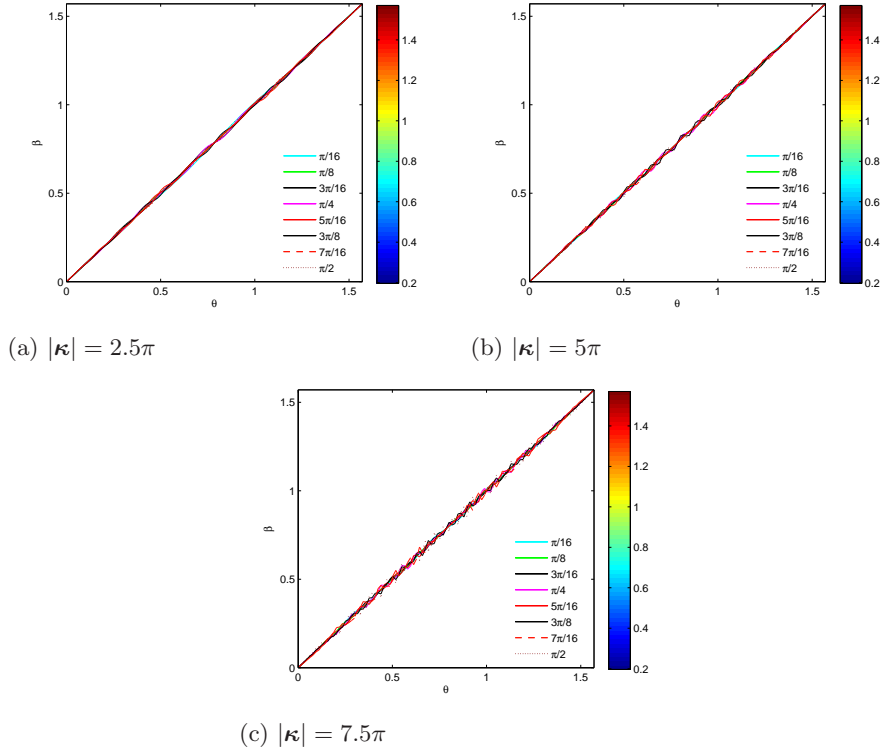


**Fig. 12:** Wave propagation angle  $\beta$  versus the wave number angle  $\theta$  at different  $|\kappa|$  with  $\tau = 0.01$ ,  $h = 0.1$  and  $N = 150$  for the Maxwell's equations.

## 8 Concluding remarks

In this paper, a sixth order energy-conserved method is first developed for the 3D time-domain Maxwell's equations. The proposed scheme can preserve all of the desired structures, including the symmetry, the five energy conservation laws, the two divergence-free fields, the three momentum conservation laws as well as the symplectic conservation law. An optimal error estimate for the proposed scheme is established with the best constant  $O(T)$  in discrete  $L^2$ -norm. Numerical results confirm our error estimate. In addition, numerical dispersion analysis show that the non-physical solution branches of the Fourier pseudo-spectral method only occur with the large wave numbers and its grid-anisotropy is direction-independent. It is well-known that the numerical computation of Maxwell's equations in metamaterials plays a very important role in seeking new designs and applications of metamaterials. Therefore, the generalization of our energy-conserved method and numerical analysis for the Maxwell's equations in metamaterials will be the subject of our future research.

## Acknowledgments

This work is supported by the National Natural Science Foundation of China (Grant Nos. 11771213 and 41504078), the National Key Research and Development Project of China (Grant No. 2016YFC0600310), the Major Projects of Natural Sciences of University in Jiangsu Province of China (Grant No. 15KJA110002) and the Priority Academic Program Development of Jiangsu Higher Education Institutions.

## Appendix:

### A A fast solver to the proposed scheme

In Ref. [6], an iterative method need be employed to solve the resulting linear equations. This leads to high computational cost. In this Appendix, a fast solver is presented to increasing computational efficiency. The idea is based on the matrix diagonalization method (see Ref. [39] and references therein) and the Fast Fourier Transform (FFT) algorithm, which is different from those of the ADI-FDTD methods (e.g., see Refs. [36, 50]) and the LOD-FDTD methods (e.g., see [23]). Below we will list the key points of this solver.

We rewrite (3.13) as

$$2\mu\mathbf{H}^{n+\frac{1}{2}} + \tau\mathbf{D}\mathbf{E}^{n+\frac{1}{2}} + \frac{c^2\tau^3}{12}\mathbf{D}^3\mathbf{E}^{n+\frac{1}{2}} + \frac{c^4\tau^5}{120}\mathbf{D}^5\mathbf{E}^{n+\frac{1}{2}} = 2\mu\mathbf{H}^n, \quad (\text{A.1})$$

$$2\epsilon\mathbf{E}^{n+\frac{1}{2}} - \tau\mathbf{D}\mathbf{H}^{n+\frac{1}{2}} - \frac{c^2\tau^3}{12}\mathbf{D}^3\mathbf{H}^{n+\frac{1}{2}} - \frac{c^4\tau^5}{120}\mathbf{D}^5\mathbf{H}^{n+\frac{1}{2}} = 2\epsilon\mathbf{E}^n. \quad (\text{A.2})$$

According to Lemma 3.3 and  $\mathcal{F}_{N_w}^{-1}\mathcal{F}_{N_w} = \mathbf{I}_{N_w}$ ,  $\mathbf{D}$  can be rewritten as

$$\mathbf{D} = \mathbf{F}^{-1}\mathbf{\Lambda}\mathbf{F}, \quad (\text{A.3})$$

where

$$\mathbf{\Lambda} = \begin{pmatrix} 0 & -\Lambda_z \otimes I_{N_y} \otimes I_{N_x} & I_{N_z} \otimes \Lambda_y \otimes I_{N_x} \\ \Lambda_z \otimes I_{N_y} \otimes I_{N_x} & 0 & -I_{N_z} \otimes I_{N_y} \otimes \Lambda_x \\ -I_{N_z} \otimes \Lambda_y \otimes I_{N_x} & I_{N_z} \otimes I_{N_y} \otimes \Lambda_x & 0 \end{pmatrix},$$

$$\mathbf{F} = \begin{pmatrix} \mathcal{F}_{N_z} \otimes \mathcal{F}_{N_y} \otimes \mathcal{F}_{N_x} & & \\ & \mathcal{F}_{N_z} \otimes \mathcal{F}_{N_y} \otimes \mathcal{F}_{N_x} & \\ & & \mathcal{F}_{N_z} \otimes \mathcal{F}_{N_y} \otimes \mathcal{F}_{N_x} \end{pmatrix}.$$

Let

$$\widetilde{\mathbf{H}}_w^{n+\frac{1}{2}} = \mathcal{F}_{N_z} \otimes \mathcal{F}_{N_y} \otimes \mathcal{F}_{N_x} \mathbf{H}_w^{n+\frac{1}{2}}, \quad \widetilde{\mathbf{H}}_w^n = \mathcal{F}_{N_z} \otimes \mathcal{F}_{N_y} \otimes \mathcal{F}_{N_x} \mathbf{H}_w^n, \quad (\text{A.4})$$

$$\widetilde{\mathbf{E}}_w^{n+\frac{1}{2}} = \mathcal{F}_{N_z} \otimes \mathcal{F}_{N_y} \otimes \mathcal{F}_{N_x} \mathbf{E}_w^{n+\frac{1}{2}}, \quad \widetilde{\mathbf{E}}_w^n = \mathcal{F}_{N_z} \otimes \mathcal{F}_{N_y} \otimes \mathcal{F}_{N_x} \mathbf{E}_w^n. \quad (\text{A.5})$$

Left-multiplying (A.1) and (A.2) with  $\widetilde{\mathbf{F}}$ , respectively, we have

$$2\mu \begin{pmatrix} \widetilde{\mathbf{H}}_x^{n+\frac{1}{2}} \\ \widetilde{\mathbf{H}}_y^{n+\frac{1}{2}} \\ \widetilde{\mathbf{H}}_z^{n+\frac{1}{2}} \end{pmatrix} + \left( \tau \mathbf{\Lambda} + \frac{c^2 \tau^3}{12} \mathbf{\Lambda}^3 + \frac{c^4 \tau^5}{120} \mathbf{\Lambda}^5 \right) \begin{pmatrix} \widetilde{\mathbf{E}}_x^{n+\frac{1}{2}} \\ \widetilde{\mathbf{E}}_y^{n+\frac{1}{2}} \\ \widetilde{\mathbf{E}}_z^{n+\frac{1}{2}} \end{pmatrix} = 2\mu \begin{pmatrix} \widetilde{\mathbf{H}}_x^n \\ \widetilde{\mathbf{H}}_y^n \\ \widetilde{\mathbf{H}}_z^n \end{pmatrix}, \quad (\text{A.6})$$

$$2\epsilon \begin{pmatrix} \widetilde{\mathbf{E}}_x^{n+\frac{1}{2}} \\ \widetilde{\mathbf{E}}_y^{n+\frac{1}{2}} \\ \widetilde{\mathbf{E}}_z^{n+\frac{1}{2}} \end{pmatrix} - \left( \tau \mathbf{\Lambda} + \frac{c^2 \tau^3}{12} \mathbf{\Lambda}^3 + \frac{c^4 \tau^5}{120} \mathbf{\Lambda}^5 \right) \begin{pmatrix} \widetilde{\mathbf{H}}_x^{n+\frac{1}{2}} \\ \widetilde{\mathbf{H}}_y^{n+\frac{1}{2}} \\ \widetilde{\mathbf{H}}_z^{n+\frac{1}{2}} \end{pmatrix} = 2\epsilon \begin{pmatrix} \widetilde{\mathbf{E}}_x^n \\ \widetilde{\mathbf{E}}_y^n \\ \widetilde{\mathbf{E}}_z^n \end{pmatrix}. \quad (\text{A.7})$$

Denoting

$$\mathbf{a}_{j,k,m} = \begin{pmatrix} 0 & -\Lambda_{zmm} & \Lambda_{ykk} \\ \Lambda_{zmm} & 0 & -\Lambda_{xjj} \\ -\Lambda_{ykk} & \Lambda_{xjj} & 0 \end{pmatrix}, \quad (\text{A.8})$$

Eqs. (A.6)-(A.7) can be rewritten into the following subsystems

$$\mathbf{A}_{j,k,m} \begin{pmatrix} \widetilde{\mathbf{H}}_{x,j,k,m}^{n+\frac{1}{2}} \\ \widetilde{\mathbf{H}}_{y,j,k,m}^{n+\frac{1}{2}} \\ \widetilde{\mathbf{H}}_{z,j,k,m}^{n+\frac{1}{2}} \\ \widetilde{\mathbf{E}}_{x,j,k,m}^{n+\frac{1}{2}} \\ \widetilde{\mathbf{E}}_{y,j,k,m}^{n+\frac{1}{2}} \\ \widetilde{\mathbf{E}}_{z,j,k,m}^{n+\frac{1}{2}} \end{pmatrix} = \mathbf{B}_{j,k,m} \begin{pmatrix} \widetilde{\mathbf{H}}_{x,j,k,m}^n \\ \widetilde{\mathbf{H}}_{y,j,k,m}^n \\ \widetilde{\mathbf{H}}_{z,j,k,m}^n \\ \widetilde{\mathbf{E}}_{x,j,k,m}^n \\ \widetilde{\mathbf{E}}_{y,j,k,m}^n \\ \widetilde{\mathbf{E}}_{z,j,k,m}^n \end{pmatrix}, \quad \begin{matrix} j = 1, \dots, N_x, \\ k = 1, \dots, N_y, \\ m = 1, \dots, N_z, \end{matrix} \quad (\text{A.9})$$

where

$$\mathbf{A}_{j,k,m} = \begin{pmatrix} 2\mu \mathbf{I}_3 & \bar{\mathbf{a}}_{j,k,m} \\ -\bar{\mathbf{a}}_{j,k,m} & 2\epsilon \mathbf{I}_3 \end{pmatrix}, \quad \mathbf{B}_{j,k,m} = \begin{pmatrix} 2\mu \mathbf{I}_3 & \\ & 2\epsilon \mathbf{I}_3 \end{pmatrix},$$

and

$$\bar{\mathbf{a}}_{j,k,m} = \tau \mathbf{a}_{j,k,m} + \frac{c^2 \tau^3}{12} \mathbf{a}_{j,k,m}^3 + \frac{c^4 \tau^5}{120} \mathbf{a}_{j,k,m}^5.$$

Since  $\mathbf{A}_{j,k,m}$  is a constant nondegenerate matrix (see Remark A.1), for a fixed  $(j, k, m)$ , we have

$$\begin{pmatrix} \widetilde{\mathbf{H}}_{x,j,k,m}^{n+\frac{1}{2}} \\ \widetilde{\mathbf{H}}_{y,j,k,m}^{n+\frac{1}{2}} \\ \widetilde{\mathbf{H}}_{z,j,k,m}^{n+\frac{1}{2}} \\ \widetilde{\mathbf{E}}_{x,j,k,m}^{n+\frac{1}{2}} \\ \widetilde{\mathbf{E}}_{y,j,k,m}^{n+\frac{1}{2}} \\ \widetilde{\mathbf{E}}_{z,j,k,m}^{n+\frac{1}{2}} \end{pmatrix} = \mathbf{A}_{j,k,m}^{-1} \mathbf{B}_{j,k,m} \begin{pmatrix} \widetilde{\mathbf{H}}_{x,j,k,m}^n \\ \widetilde{\mathbf{H}}_{y,j,k,m}^n \\ \widetilde{\mathbf{H}}_{z,j,k,m}^n \\ \widetilde{\mathbf{E}}_{x,j,k,m}^n \\ \widetilde{\mathbf{E}}_{y,j,k,m}^n \\ \widetilde{\mathbf{E}}_{z,j,k,m}^n \end{pmatrix} := \mathcal{A}_{j,k,m} \begin{pmatrix} \widetilde{\mathbf{H}}_{x,j,k,m}^n \\ \widetilde{\mathbf{H}}_{y,j,k,m}^n \\ \widetilde{\mathbf{H}}_{z,j,k,m}^n \\ \widetilde{\mathbf{E}}_{x,j,k,m}^n \\ \widetilde{\mathbf{E}}_{y,j,k,m}^n \\ \widetilde{\mathbf{E}}_{z,j,k,m}^n \end{pmatrix}, \quad (\text{A.10})$$



Solving the above equations gives  $\widetilde{\mathbf{H}}_w^{n+\frac{1}{2}}$  and  $\widetilde{\mathbf{E}}_w^{n+\frac{1}{2}}$ . Using the relations  $\mathbf{H}_w^{n+1} = 2\mathcal{F}_{N_z}^{-1} \otimes \mathcal{F}_{N_y}^{-1} \otimes \mathcal{F}_{N_x}^{-1} \widetilde{\mathbf{H}}_w^{n+\frac{1}{2}} - \mathbf{H}_w^n$  and  $\mathbf{E}_w^{n+1} = 2\mathcal{F}_{N_z}^{-1} \otimes \mathcal{F}_{N_y}^{-1} \otimes \mathcal{F}_{N_x}^{-1} \widetilde{\mathbf{E}}_w^{n+\frac{1}{2}} - \mathbf{E}_w^n$  yields the solutions  $\mathbf{H}_w^{n+1}$  and  $\mathbf{E}_w^{n+1}$ . Note that the matrix  $\mathcal{A}$  in Eq. (A.10) need only be computed once and the Fast Fourier Transform (FFT) algorithm can be applied to the above process.

**Remark A.1.** Note that there exists an orthogonal matrix  $\mathbf{O}$  such that

$$\mathbf{a}_{12} = \mathbf{O}^T \widetilde{\mathbf{\Lambda}} \mathbf{O}, \quad \widetilde{\mathbf{\Lambda}} = \text{diag}\left(\lambda_1, \lambda_2, \lambda_3\right), \quad \lambda_1 = 0, \quad \lambda_{2,3} = \pm \sqrt{-\Lambda_{xjj}^2 - \Lambda_{ykk}^2 - \Lambda_{zmm}^2},$$

which further implies that

$$\bar{\mathbf{a}}_{12} = \mathbf{O}^T \widetilde{\mathbf{\Lambda}}_\tau \mathbf{O}, \quad \widetilde{\mathbf{\Lambda}}_\tau = \text{diag}\left(\tilde{\lambda}_1, \tilde{\lambda}_2, \tilde{\lambda}_3\right), \quad \tilde{\lambda}_1 = 0, \quad \tilde{\lambda}_{2,3} = \tau \lambda_{2,3} + \frac{c^2 \tau^3}{12} \lambda_{2,3}^3 + \frac{c^4 \tau^5}{120} \lambda_{2,3}^5.$$

Thus, it is clear to see that

$$\begin{aligned} |\mathbf{A}| &= \left| \begin{pmatrix} \mathbf{O}^T & \\ & \mathbf{O}^T \end{pmatrix} \begin{pmatrix} 2\mu \mathbf{I}_{3 \times 3} & \widetilde{\mathbf{\Lambda}}_\tau \\ -\widetilde{\mathbf{\Lambda}}_\tau & 2\epsilon \mathbf{I}_{3 \times 3} \end{pmatrix} \begin{pmatrix} \mathbf{O} & \\ & \mathbf{O} \end{pmatrix} \right| \\ &= \left| \begin{pmatrix} 2\mu \mathbf{I}_{3 \times 3} & \widetilde{\mathbf{\Lambda}}_\tau \\ 2\epsilon \mathbf{I}_{3 \times 3} + \frac{1}{2\mu} \widetilde{\mathbf{\Lambda}}_\tau^2 \end{pmatrix} \right| \neq 0. \end{aligned}$$

## References

- [1] N. Anderson and A.M. Arthurs. Helicity and variational principles for Maxwell's equations. *Int. J. Electron.*, 54:861–864, 1983.
- [2] U.M. Ascher and R.I. McLachlan. Multisymplectic box schemes and the Korteweg-de Vries equation. *Appl. Numer. Math.*, 48:255–269, 2004.
- [3] J.P. Bérenger. A perfectly matched layer for the absorption of electromagnetic waves. *J. Comput. Phys.*, 114:185–200, 1994.
- [4] J.P. Bérenger. Three-dimensional perfectly matched layer for the absorption of electromagnetic waves. *J. Comput. Phys.*, 127:363–379, 1996.
- [5] J.X. Cai, J.L. Hong, Y.S. Wang, and Y.Z. Gong. Two energy-conserved splitting methods for three-dimensional time-domain Maxwell's equations and the convergence analysis. *SIAM. J. Numer. Anal.*, 53:1918–1940, 2015.
- [6] J.X. Cai, Y.S. Wang, and Y.Z. Gong. Numerical analysis of AVF methods for three-dimensional time-domain Maxwell's equations. *J. Sci. Comput.*, 66:141–176, 2016.
- [7] W.J. Cai, Y.S. Wang, and Y.Z. Song. Numerical dispersion analysis of a multi-symplectic scheme for the three dimensional Maxwell's equations. *J. Comput. Phys.*, 234:330–352, 2013.
- [8] C. Canuto and A. Quarteroni. Approximation results for orthogonal polynomials in Sobolev spaces. *Math. Comput.*, 38:67–86, 1982.
- [9] E. Celledoni, V. Grimm, R.I. McLachlan, D. O'Neale, B. Owren, and G.R.W. Quispel. Preserving energy resp. dissipation in numerical PDEs using the “average vector field” method. *J. Comput. Phys.*, 231:6770–6789, 2012.

- [10] E. Celledoni, R.I. McLachlan, B. Owren, and G.R.W Quispel. Energy-preserving integrators and the structure of B-series. *Found. Comput. Math.*, 2010.
- [11] P. Chartier, E. Hairer, and G. Vilmart. A substitution law for B-series vector fields. *INRIA report*, 2005.
- [12] J.B. Chen and M.Z. Qin. Multi-symplectic Fourier pseudospectral method for the nonlinear Schrödinger equation. *Electr. Trans. Numer. Anal.*, 12:193–204, 2001.
- [13] W.B. Chen, X.J. Li, and D. Liang. Energy-conserved splitting FDTD methods for Maxwell’s equations. *Numer. Math.*, 108:445–485, 2008.
- [14] W.B. Chen, X.J. Li, and D. Liang. Energy-conserved splitting finite-difference time-domain methods for Maxwell’s equations in three dimensions. *SIAM. J. Numer. Anal.*, 48:1530–1554, 2010.
- [15] B. Cockburn, F. Li, and C.W. Shu. Locally divergence-free discontinuous Galerkin methods for the Maxwell equations. *J. Comput. Phys.*, 194:588–610, 2004.
- [16] M. Dahlby and B. Owren. A general framework for deriving integral preserving numerical methods for PDEs. *SIAM J. Sci. Comput.*, 33:2318–2340, 2011.
- [17] K. Feng and M.Z. Qin. *Symplectic geometric algorithms for Hamiltonian systems*. Springer and Zhejiang Science and Technology Publishing House, Heidelberg Hangzhou, 2010.
- [18] L.P. Gao and B. Zhang. Optimal error estimates and modified energy conservation identities of the ADI-FDTD scheme on staggered grids for 3D Maxwell’s equations. *Sci. Chin. Math*, 56:1705–1726, 2013.
- [19] Y.Z. Gong, J.X. Cai, and Y.S. Wang. Multi-symplectic Fourier pseudospectral method for the Kawahara equation. *Commun. Comput. Phys.*, 16:35–55, 2014.
- [20] E. Hairer, C. Lubich, and G. Wanner. *Geometric Numerical Integration: Structure-Preserving Algorithms for Ordinary Differential Equations*. Springer-Verlag, Berlin, 2nd edition, 2006.
- [21] T. Hirono, W. Lui, S. Seki, and Y. Yoshikuni. A three-dimensional fourth-order finite-difference time-domain scheme using a symplectic integrator propagator. *IEEE Trans. Microwave Theory Tech.*, 49:1640–1648, 2001.
- [22] J.L. Hong, L.H. Ji, and L.H. Kong. Energy-dissipations splitting finite-difference time-domain method for Maxwell equations with perfectly matched layers. *J. Comput. Phys.*, 269:201–214, 2014.
- [23] J. Yamauchi J. Shibayama, M. Muraki and H. Nakano. Efficient implicit fdtd algorithm based on locally one-dimensional scheme. *Electron. Lett.*, 41:1046–1047, 2005.
- [24] J. D. Jackson. *Classical electrodynamics*. John Wiley & Sons Inc., New York, third ed edition, 1998.
- [25] L.H. Kong, J.L. Hong, and J.J. Zhang. Splitting multisymplectic integrators for Maxwells equations. *J. Comput. Phys.*, 229:4259–4278, 2010.
- [26] B. Leimkuhler and S. Reich. *Simulating Hamiltonian dynamics*. Cambridge University Press, Cambridge, 2004.

- [27] H.C. Li, Y.S. Wang, and M.Z. Qin. A sixth order averaged vector field method. *J. Comput. Math.*, 34:479–498, 2016.
- [28] D. Liang and Q. Yuan. The spatial fourth-order energy-conserved S-FDTD scheme for Maxwell’s equations. *J. Comput. Phys.*, 243:344–364, 2013.
- [29] Q.H. Liu. The PSTD algorithm: a time-domain method requiring only two cells per wavelength. *Microw. Opt. Technol. Lett.*, 15:158–165, 1997.
- [30] J.E. Marsden, G.W. Patrick, and S. Shkoller. Multisymplectic geometry, variational integrators, and nonlinear PDEs. *Comm. Math. Phys.*, 199:351–395, 1998.
- [31] J.E. Marsden and A. Weinstein. The Hamiltonian structure of the Maxwell-Vlasov equations. *Physica D*, 4:394–406, 1982.
- [32] R.I. McLachlan, G.R.W. Quispel, and N. Robidoux. Geometric integration using discrete gradients. *Philos. Trans. R. Soc. A.*, 357:1021–1046, 1999.
- [33] P. Monk. *Finite element methods for Maxwell’s equations*. Clarendon press, Oxford, edition, 2003.
- [34] P. Monk and E. Süli. A convergence analysis of Yee’s scheme on nonuniform grids. *SIAM J. Numer. Anal.*, 31:393–412, 1994.
- [35] C.D. Munz, P. Ommes, and R. Schneider et al. Divergence correction techniques for Maxwell solvers based on a hyperbolic model. *J. Comput. Phys.*, 161:484–511, 2000.
- [36] T. Namiki. A new FDTD algorithm based on alternating-direction implicit method. *IEEE Trans. Microw. Theory Tech.*, 47:2003–2007, 1999.
- [37] G.R.W. Quispel and D.I. McLaren. A new class of energy-preserving numerical integration methods. *J. Phys. A: Math. Theor.*, 41:045206, 2008.
- [38] J.S. Shang. High-order compact-difference schemes for time-dependent Maxwell equations. *J. Comput. Phys.*, 153:312–333, 1999.
- [39] J. Shen and T. Tang. *Spectral and High-Order Methods with Applications*. Science Press, Beijing, 2006.
- [40] T.W.H. Sheu, Y.W. Chung, J.H. Li, and Y.C. Wang. Development of an explicit non-staggered scheme for solving three-dimensional Maxwell’s equations. *Comput. Phys. Commun.*, 207:258–273, 2016.
- [41] A. Stern, Y. Tong, M. Desbrun, and J.E. Marsden. *Geometric computational electrodynamics with variational integrators and discrete differential forms*, In: *Geometry, Mechanics, and Dynamics*, pp. 437–475. Springer, New York, 2015.
- [42] H.L. Su, M.Z. Qin, and R. Scherer. A multisymplectic geometry and a multisymplectic scheme for Maxwell’s equations. *Int. J. Pure. Appl. Math.*, 34:1–17, 2007.
- [43] Y.J. Sun and P.S.P. Tse. Symplectic and multi-symplectic numerical methods for Maxwell’s equations. *J. Comput. Phys.*, 230:2076–2094, 2011.
- [44] A. Taflove and S.C. Hagness. *Computational electrodynamics*. Artech House, Boston, 2005.

- [45] L.N. Trefethen. Group velocity in finite difference schemes. *SIAM. Rev.*, 24:113–136, 1982.
- [46] G.B. Whitham. *Linear and nonlinear waves*. John Wiley & Sons Inc., New York, 1999.
- [47] K.S. Yee. Numerical solution of initial boundary value problems involving Maxwell’s equations in isotropic media. *IEEE Trans. Antennas Propag.*, 14:302–307, 1966.
- [48] A. Yefet and P.G. Petropoulos. A non-dissipative staggered fourth-order accurate explicit finite difference scheme for the time-domain maxwell’s equation. *J. Comput. Phys.*, 168:286–315, 2001.
- [49] S. Zhao and G.W. Wei. High-order FDTD methods via derivative matching for Maxwell’s equations with material interfaces. *J. Comput. Phys.*, 200:60–103, 2004.
- [50] F.H. Zhen, Z.Z. Chen, and J.Z. Zhang. Toward the development of a three-dimensional unconditionally stable finite-difference time-domain method. *IEEE. Trans. Microw. Theory Tech.*, 48:1550–1558, 2000.
- [51] H.J. Zhu, S.H. Song, and Y.M. Chen. Multi-symplectic wavelet collocation method for Maxwell’s equations. *Adv. Appl. Math. Mech.*, 3:663–688, 2011.